Article

Cell

Bypassing Negative Epistasis on Yield in Tomato Imposed by a Domestication Gene

Graphical Abstract

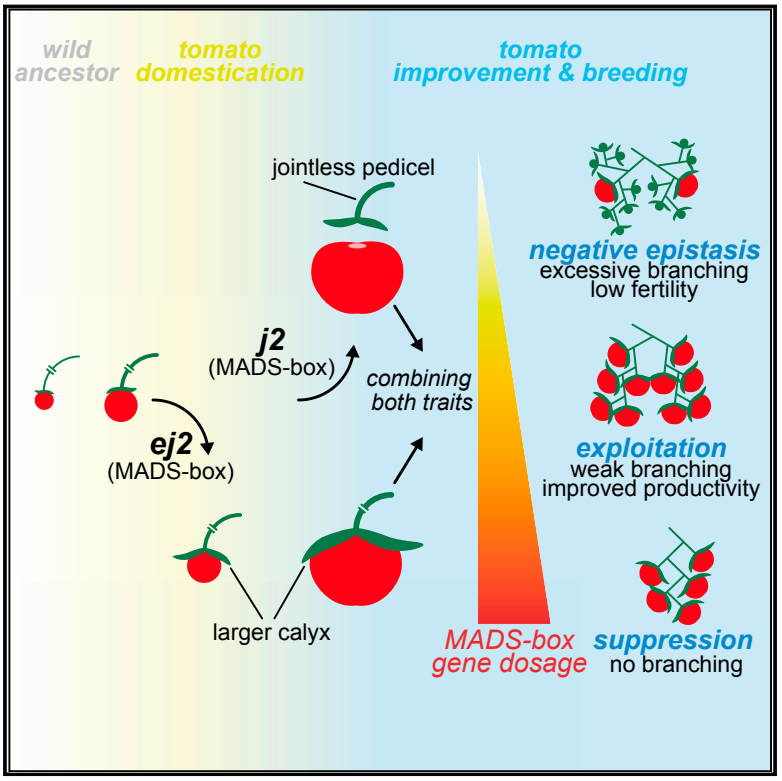

Highlights

- Mutations in two MADS-box genes were selected in tomato domestication and breeding
- Interaction of the alleles caused extreme inflorescence branching and sterility
- Natural and gene-edited MADS-box alleles provide a range of inflorescence types
- Dosage from selected alleles allows improved inflorescence architecture and yield

Authors

Sebastian Soyk, Zachary H. Lemmon, Matan Oved, ..., Dani Zamir, Yuval Eshed, Zachary B. Lippman

Correspondence

lippman@cshl.edu

In Brief

Why did a crop domestication gene hinder breeding with a modern breeding gene responsible for the beneficial "jointless" trait in tomato, and how can this genetic interaction be overcome and exploited?

Soyk et al., 2017, Cell *169*, 1142–1155
June 1, 2017
http://dx.doi.org/10.1016/j.cell.2017.04.032

CellPress

Cell

Article

Bypassing Negative Epistasis on Yield in Tomato Imposed by a Domestication Gene

Sebastian Soyk,[1,10] Zachary H. Lemmon,[1,10] Matan Oved,[2] Josef Fisher,[2] Katie L. Liberatore,[1,3,8] Soon Ju Park,[4] Anna Goren,[5] Ke Jiang,[1,9] Alexis Ramos,[6] Esther van der Knaap,[6] Joyce Van Eck,[7] Dani Zamir,[2] Yuval Eshed,[5] and Zachary B. Lippman[1,3,11,*]

[1]Cold Spring Harbor Laboratory, Cold Spring Harbor, NY 11724, USA
[2]Faculty of Agriculture, Hebrew University of Jerusalem, Rehovot 76100, Israel
[3]Watson School of Biological Sciences, Cold Spring Harbor Laboratory, Cold Spring Harbor, NY 11724, USA
[4]Division of Biological Sciences and Research Institute for Basic Science, Wonkwang University, Iksan, Jeonbuk 54538, Rep. of Korea
[5]Department of Plant and Environmental Sciences, Weizmann Institute of Science, Rehovot 76100, Israel
[6]Institute of Plant Breeding, Genetic & Genomics, University of Georgia, Athens, GA 30602, USA
[7]The Boyce Thompson Institute, Ithaca, NY 14853, USA
[8]Present address: Cereal Disease Laboratory, US Department of Agriculture, St. Paul, MN 55108, USA
[9]Present address: Dow AgroSciences, Indianapolis, IN 46268, USA
[10]These authors contributed equally
[11]Lead Contact
*Correspondence: lippman@cshl.edu
http://dx.doi.org/10.1016/j.cell.2017.04.032

SUMMARY

Selection for inflorescence architecture with improved flower production and yield is common to many domesticated crops. However, tomato inflorescences resemble wild ancestors, and breeders avoided excessive branching because of low fertility. We found branched variants carry mutations in two related transcription factors that were selected independently. One founder mutation enlarged the leaf-like organs on fruits and was selected as fruit size increased during domestication. The other mutation eliminated the flower abscission zone, providing "jointless" fruit stems that reduced fruit dropping and facilitated mechanical harvesting. Stacking both beneficial traits caused undesirable branching and sterility due to epistasis, which breeders overcame with suppressors. However, this suppression restricted the opportunity for productivity gains from weak branching. Exploiting natural and engineered alleles for multiple family members, we achieved a continuum of inflorescence complexity that allowed breeding of higher-yielding hybrids. Characterizing and neutralizing similar cases of negative epistasis could improve productivity in many agricultural organisms.

INTRODUCTION

The architectures of plant reproductive shoot systems—inflorescences—are major determinants of crop yield, and modified inflorescence complexity was a recurring target during crop domestication and improvement (Meyer and Purugganan, 2013). Prominent examples include the cereal crops barley, maize, rice, and wheat, for which humans selected variants with greater branching to increase flower and grain production (Boden et al., 2015; Doebley et al., 1997; Huang et al., 2009; Ramsay et al., 2011). Yet for many crops, particularly fruit-bearing species such as grape and tomato, inflorescence architecture has changed little from wild ancestors and, therefore, has been underexploited in breeding (Mullins et al., 1992; Peralta and Spooner, 2005).

Variation in inflorescence architecture is based on changes in the activity of meristems, small groups of stem cells located at the tips of shoots (Kyozuka et al., 2014; Park et al., 2014a). During the transition to flowering, vegetative meristems gradually mature to a reproductive state and, depending on the species, terminate immediately in a flower or give rise to a variable number of new inflorescence meristems that become additional flowers or flower-bearing branches. In domesticated tomato (*Solanum lycopersicum*) and its wild progenitor *S. pimpinellifolium*, a new inflorescence meristem emerges at the flank of each previous meristem. Several reiterations of this process give rise to inflorescences with multiple flowers arranged in a zigzag pattern, resulting in the familiar "tomatoes-on-the-vine" architecture (Figure 1A) (Park et al., 2012).

Despite a rich resource of wild relatives that develop weakly branched inflorescences with high fertility, improving tomato inflorescence architecture to boost flower production and yield has remained challenging due to genetic incompatibilities and the challenge of transferring complex polygenic traits (Lemmon et al., 2016; Lippman et al., 2008; Macarthur and Chiasson, 1947). Another potentially valuable source of inflorescence variation is rare natural and induced highly branched mutants in domesticated germplasm. We previously showed that branching in one of these variants and in a related wild species is due to an extended meristem maturation schedule, which allows additional inflorescence meristems to form (Lemmon et al., 2016; Park et al., 2012). These findings suggested that subtle modification of meristem maturation could provide beneficial changes in

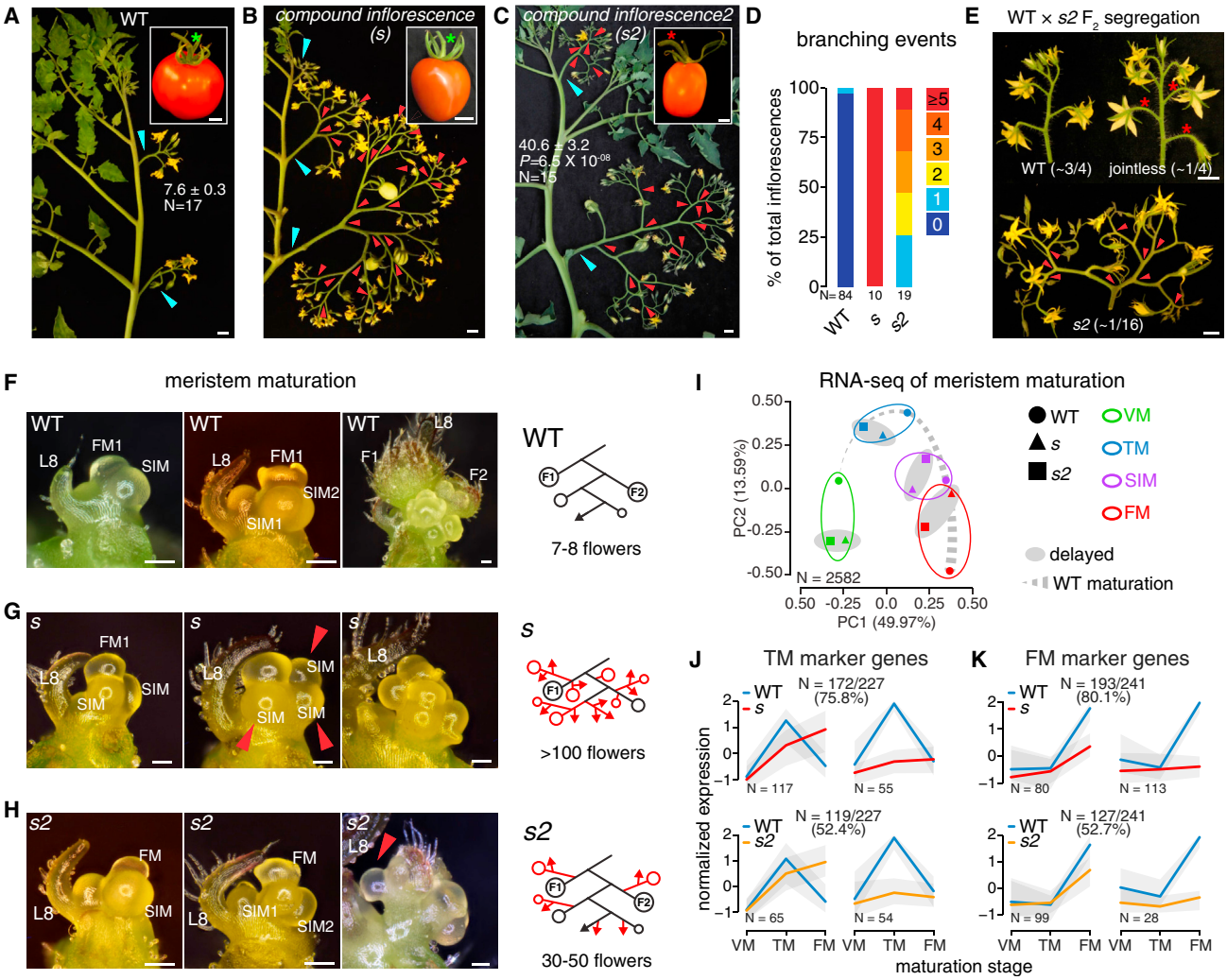

Figure 1. The *s2* Inflorescence Architecture Variant Branches Due to Delayed Meristem Maturation

(A) Typical WT tomato plant with unbranched, multi-flowered inflorescences and jointed pedicels (green asterisk). Numbers in (A)–(C) indicate flowers per inflorescence (mean ± SEM, N = number of inflorescences). Cyan arrowheads indicate successive inflorescences. *P*, two-tailed, two-sample t test compared to WT.

(B) The highly branched inflorescences and jointed pedicels of *s* mutants. Red arrowheads indicate branch points.

(C) *s2* mutant with moderately branched inflorescences and jointless pedicels (red asterisk).

(D) Quantification of inflorescence branching events in WT, *s*, and *s2*.

(E) Phenotypic classes in a WT × *s2* F_2 population. The segregation ratio for the jointless pedicel phenotype and the branched inflorescence phenotype (*s2*) is given. Red asterisks mark jointless pedicels. Scale bars in (A)–(C) and (E), 1 cm.

(F–H) The transition meristem (TM), sympodial inflorescence meristem (SIM), and floral meristem (FM) from WT (F), *s* (G), and *s2* (H). Scale bars in (F) –(H) represent 100 μm. L, leaf. F, flower. Schematics depict developing inflorescences. Lines, internodes; circles, FMs/flowers; arrowheads, SIMs. Overproliferating branches are indicated in red.

(I) PCA of 2,582 dynamically expressed genes in the vegetative meristem (VM), TM, SIM, and FM of WT, *s*, and *s2*, determined by RNA-seq.

(J and K) Expression (*z*-score normalized) of TM (J) and FM (K) marker genes in the vegetative (VM) meristem, TM and FM stage of meristem maturation of WT and mutant (*s* and *s2*). Cluster of genes with moderately (left) and strongly (right) delayed expression pattern are shown. Colored lines indicate median expression, with gray area representing the 5th and 95th quantile.

See also Figures S1 and S2 and Table S1.

inflorescence architecture (Park et al., 2014a). Yet breeders typically select against even moderate branching, primarily due to imbalances in source-sink relationships that cause flower abortion and low fruit production, especially in large-fruited varieties (Stephenson, 1981).

In this study, we explored a new class of branched variants from a large core collection and discovered mutations in two closely related MADS-box transcription factor genes, one of which arose during domestication and the other within the last century of crop improvement. Each mutation was selected

separately for improved flower morphology and fruit retention traits. However, redundant roles in meristem maturation caused undesirable branching upon combining both mutations. Breeders overcame this negative epistasis by selecting suppressors of branching, but in so doing, they limited the potential to improve flower production through weak branching. By dissecting this interaction, we discovered a dosage relationship among natural and gene-edited mutations in multiple regulators of meristem maturation. Combining these mutations in homozygous and heterozygous states allowed us to create a quantitative range of inflorescence types and develop weakly branched hybrids with higher flower and fruit production.

RESULTS

The *s2* Variants Produce Branched Inflorescences and Flowers with Jointless Pedicels

To explore the challenges with improving tomato inflorescences, we screened a core collection of 4,193 wild and domesticated accessions for deviation from the typical inflorescence architecture of multiple flowers arranged along a single branch (Figure 1A) (https://unity.phenome-networks.com, see STAR Methods). We previously reported 23 extremely branched accessions that were all defective in the gene *COMPOUND INFLORESCENCE* (*S*, homolog of *Arabidopsis WUSCHEL-RELATED HOMEOBOX 9*, *WOX9*) (Figure 1B) (Lippman et al., 2008). However, we also found three rare variants not allelic to *s* that branched less frequently and also lacked the abscission zone on the stems (pedicels) of flowers known as the "joint" (Figures 1C, 1D, and S1A–S1F). Searching other germplasm sources provided one additional branched jointless mutant derived from an X-ray mutagenesis (Figures S1C and S1F) (Stubbe, 1972). Crosses among all four accessions failed to complement (Figures S1G–S1I). Thus, we collectively named these accessions *compound inflorescence 2* (*s2*) and designated one accession as a reference (LA4371, see STAR Methods).

An analysis of higher-order mutants between *s* and *s2* showed an additive genetic relationship, indicating that the gene(s) underlying *s2* function separately from the *S* gene (Figures 1C and S1J). We noted during the generation of *s s2* plants that *s2* segregated at a ratio of ~1/16 (Figure 1E), suggesting that two unlinked recessive mutations underlie *s2* phenotypes. Consistent with this, jointless plants (unbranched and branched) segregated as a single recessive mutation. This jointless trait resembled two classical *jointless-2* (*j2*) mutants reported 50 years ago. The original *j2* was discovered in the unbranched wild tomato species *S. cheesmaniae* from the Galapagos Islands (Rick, 1956a). A second allele arose spontaneously in an agricultural field, but this mutation was also associated with inflorescence branching that caused excessive flower production and poor fruit set due to epistatic interactions with the domesticated germplasm (Reynard, 1961; Rick, 1956b). Breeders selected and utilized unbranched *j2* because it reduced fruit dropping and enabled large-scale machine harvesting of processing tomatoes while maintaining good fruit set (Zahara and Scheuerman, 1988). Notably, the jointless phenotype of *s2* was allelic to *j2* (Figure S1K), and we failed to find *s2* plants with normal pedicels, suggesting that branching required the *j2* mutation. We therefore designated the second locus *enhancer-of-jointless2* (*ej2*).

To better understand the developmental basis of *s2* branching, we examined stages of meristem maturation during early inflorescence development. Tomato inflorescences develop according to the sympodial growth program (Park et al., 2014a), in which each vegetative meristem matures into a transition meristem (TM) and terminates in a floral meristem (FM) that produces the first flower of the inflorescence. Additional flowers arise from iterative formation of specialized axillary (sympodial) inflorescence meristems (SIM), resulting in a multi-flowered inflorescence (Figure 1F). In *s* mutants, both TM and SIM maturation are severely delayed, allowing multiple SIMs to form at each cycle (Figure 1G) (Lippman et al., 2008; Park et al., 2012). Additional SIMs also formed in *s2* plants, but fewer than in *s* (Figure 1H). To determine if *s2* was delayed in maturation, we performed RNA-seq on sequential *s2* meristem maturation stages and compared transcriptome dynamics with existing maturation profiles for *s* and wild-type (WT) (see STAR Methods). A principal component analysis (PCA) using 2,582 maturation marker genes (Lemmon et al., 2016) showed that meristem maturation in *s2* was delayed like in *s*, and subsets of TM and FM marker genes showed that this delay was weaker than *s* consistent with less branching in *s2* inflorescences (Figures 1I–1K and S2).

Mutations in Two Related MADS-Box Genes Cause *s2* Branching

The *j2* mutant was previously mapped to the centromere of chromosome 12, but poor recombination prevented identification of the responsible gene (Budiman et al., 2004; Yang et al., 2005). To clone the genes underlying *j2* and *ej2*, we generated two F_2 populations from crossing *s2* with the jointed (*J2/J2*) cultivar M82 and the wild ancestor of tomato, *S. pimpinellifolium*. In the intra-species F_2 population, *s2* plants segregated at the expected ratio of ~1/16, but this segregation was substantially lower in the *S. pimpinellifolium* population, suggesting unknown modifier loci can suppress *s2* branching (Figures S3A–S3C). To map *j2* and *ej2* simultaneously, we performed genome sequencing on pools of DNA from *s2*, *j2*, and WT F_2 segregating plants (see STAR Methods). Comparing SNP ratios between *s2* and WT pools in both populations revealed a region near the bottom of chromosome 3 and the centromere of chromosome 12 with a strong bias for SNPs from the *s2* parent (Figures 2A, S3D, and S3E). SNP ratios between *s2* and *j2* revealed a bias only on chromosome 3. These results confirmed that *j2* is located near the chromosome 12 centromere and revealed that *ej2* resides on chromosome 3.

MADS-box transcription factors are known to contribute to pedicel abscission zone development in tomato (Liu et al., 2014; Mao et al., 2000; Nakano et al., 2012; Shalit et al., 2009). The *jointless1* mutant (*j1*) was mapped to chromosome 11 and was found to be mutated in a homolog of the *Arabidopsis* MADS-box flowering regulator *SHORT VEGETATIVE PHASE* (*SVP*) (Mao et al., 2000). We therefore searched the ~6 Mbp *j2* mapping interval for MADS-box genes, and among the 164 genes in this region, we found only one candidate, *Solyc12g038510*, a homolog of the *Arabidopsis* floral organ identity MADS-box gene *SEPALLATA4* (*SEP4*) (Figure 2B) (Ditta et al., 2004). Previous

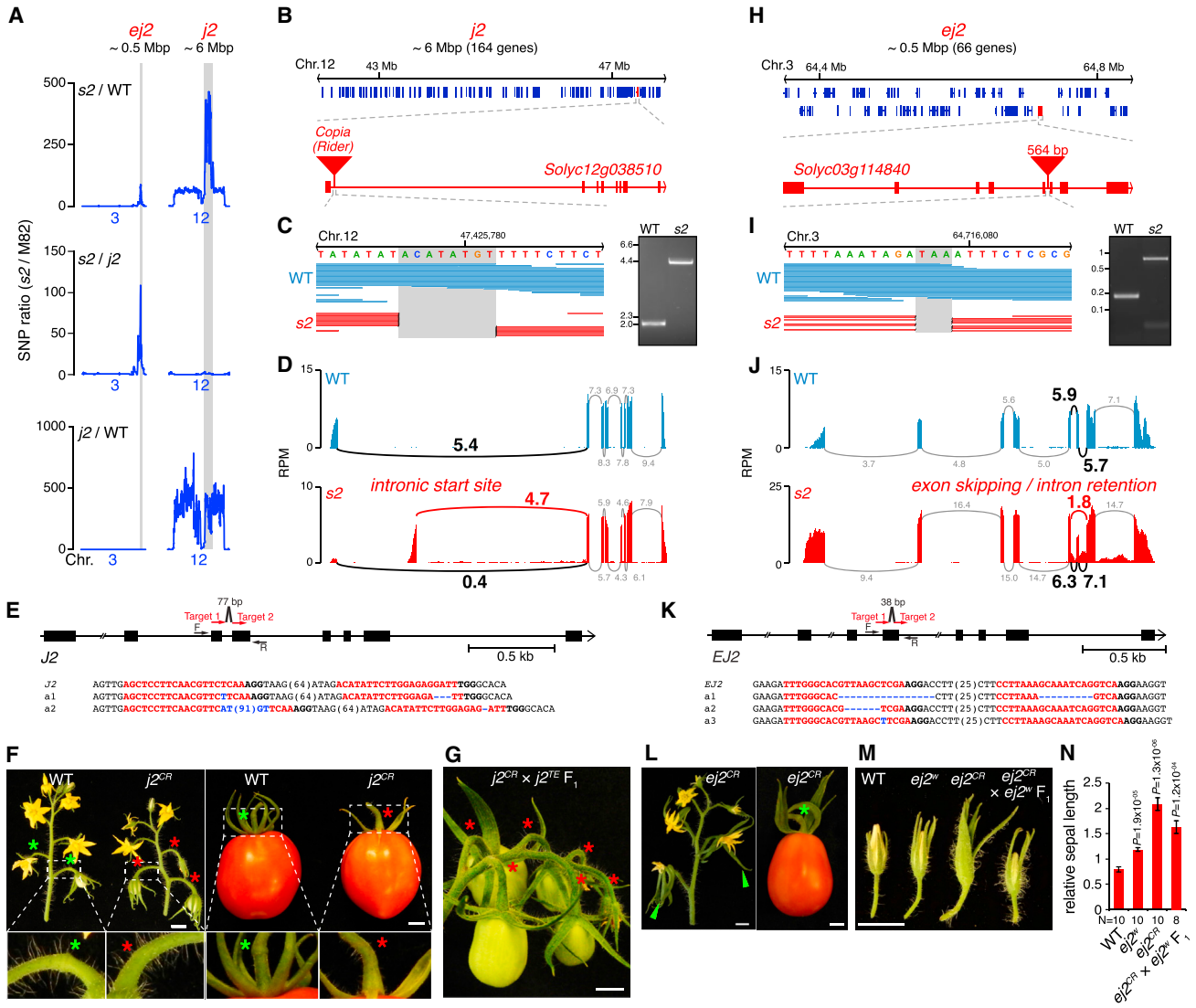

Figure 2. Mutations in Two *SEPALLATA* MADS-Box Genes Cause *s2* Branching

(A) Mapping-by-sequencing of *s2*. Ratio of SNP-ratios (*s2*/M82) between different pools of segregating phenotypic classes (top: *s2*/WT; middle: *s2*/*j2*; bottom: *j2*/WT) is shown for chromosome 3 and 12.

(B) The *j2* mapping interval includes the *SEP4* homolog *Solyc12g038510*.

(C) Genomic sequencing reads (left) and PCR (right) showing a *Copia*-like *Rider* transposon insertion in the first intron of *Solyc12g038510* in *s2* mutants.

(D) Sashimi plots of *Solyc12g038510* RNA-seq reads in WT (top) and *s2* (bottom) floral meristems. An intronic transcriptional start site leads to out-of-frame *Solyc12g038510* transcripts in *s2* mutants. Numbers indicate reads per million (RPM) supporting splice-junctions, and alternative *s2* splicing is highlighted in red.

(E) Generation of $j2^{CR}$ null mutations by CRISPR/Cas9 using two single-guide RNAs (sgRNA, target1, and target2; red arrows). Black arrows indicate forward (F) and reverse (R) primers used for genotyping and sequencing. Sequences of $j2^{CR}$ allele 1 (a1) and a2 are shown. sgRNA targets and protospacer-adjacent motif (PAM) are indicated in red and bold font, respectively, and deletions by blue dashes. Insertions are indicated in blue, and sequence gap length is shown in parentheses.

(F) Unbranched inflorescences and fruits from WT and $j2^{CR}$ mutants showing WT jointed (green asterisks) and $j2^{CR}$ jointless (red asterisks) pedicels.

(G) Complementation test between $j2^{CR}$ and $j2^{TE}$ (jointless pedicels; red asterisks).

(H) The *ej2* mapping interval includes the *SEP4* homolog *Solyc03g114840*.

(I) Genomic sequencing reads (left) and PCR (right) in *s2* mutants, revealing a 564 bp insertion in the fifth intron of *Solyc03g114840*.

(J) Sashimi plots, as in (D), for *Solyc03g114840* RNA-seq reads in WT and *s2* floral meristems, indicating partial exon skipping and intron retention in *s2* mutants.

(K) Generation of $ej2^{CR}$ null mutations by CRISPR/Cas9.

(L) Unbranched $ej2^{CR}$ mutant inflorescences with extremely long sepals (green arrowheads) and pear-shaped fruits. Scale bars, 1 cm.

(M) Unopened flowers showing that the weak natural $ej2^{w}$ allele causes longer sepals and fails to complement $ej2^{CR}$.

(N) Quantification of relative sepal length (sepal length/petal length ± SEM, N, number of flowers) for genotypes in (M). *P*, two-tailed, two-sample t test compared to WT.

See also Figure S3 and STAR Methods.

transcriptional silencing of *Solyc12g038510* resulted in jointless pedicels, but it was suggested that *Solyc12g038510* and *J2* were different genes because the published *j2* mapping interval did not coincide with *Solyc12g038510*, likely from unreliable centromeric marker resolution (Budiman et al., 2004; Liu et al., 2014). However, our genomic sequencing of *s2* and *j2* mutants exposed a *Copia*-like *Rider*-type transposable element (TE) in the first intron of *Solyc12g038510* that was absent in WT (Figure 2C). Furthermore, our *s2* RNA-seq revealed that most *Solyc12g038510* transcripts initiated in the first intron, resulting in an early nonsense mutation (Figures 2D and S3H). To validate that *Solyc12g038510* is *J2,* we used CRISPR/Cas9 to engineer loss-of-function mutations, and the resulting $j2^{CR}$ plants developed jointless unbranched inflorescences (Figures 2E and 2F). Moreover, progeny from crossing $j2^{CR}$ with *s2*-derived *j2* had jointless and unbranched inflorescences (Figure 2G), and sequencing *Solyc12g038510* in the original *j2 S. cheesmaniae* accession revealed an early stop codon (Figures S3F–S3H). Thus, the *SEP4* gene *Solyc12g038510* is *J2,* and two natural mutations arose independently (hereafter designated $j2^{TE}$ and $j2^{stop}$) (Reynard, 1961; Rick, 1956a).

Both *j2* and *ej2* are required for *s2* branching, suggesting that the underlying genes function redundantly, similar to *SEP* genes in *Arabidopsis* that control floral organ identity (Ditta et al., 2004; Pelaz et al., 2000). We searched the 66 genes in the 500 kbp *ej2* mapping interval for MADS-box genes and found the tandemly arranged *Solyc03g114830* and *Solyc03g114840* (Figure 2H). *Solyc03g114830* is a homolog of *Arabidopsis FRUITFULL* and knockdown of this gene causes subtle fruit-ripening defects (Bemer et al., 2012). Our genomic sequencing of *s2* mutants did not reveal any *Solyc03g114830* coding or noncoding SNPs or large indels, and *s2* fruits ripened normally. In contrast, *Solyc03g114840* is another homolog of *SEP4*, and we found a 564 bp insertion in the 5th intron of *s2* mutants, which was absent in WT (Figure 2I). Notably, RNA-seq reads from *s2* revealed a third of *Solyc03g114840* transcripts was misspliced, suggesting that the insertion caused a partial loss of function (Figure 2J). To test this and uncover the phenotypic consequences of strong loss of *EJ2* function, we engineered new alleles with CRISPR/Cas9 and found $ej2^{CR}$ inflorescences were unbranched, but the sepals (outermost leaf-like organs of the flowers) were exceptionally large and fruits were pear-shaped (Figures 2K and 2L). To determine if the original *ej2* mutation impacted flower or fruit morphology, we backcrossed *ej2* into M82 and measured relative sepal length (defined by sepal/petal length ratio). Notably, whereas there was no obvious change in fruit shape or size, *ej2* sepals were 50% longer than WT but shorter than $ej2^{CR}$, consistent with a weak allele (Figures 2M, 2N, and S3I). Importantly, flowers of F_1 progeny from crossing *ej2* and $ej2^{CR}$ also developed long sepals. Thus, *Solyc03g114840* is *EJ2,* and the natural *ej2* mutation is a weak loss-of-function allele (hereafter designated $ej2^{w}$).

Finally, we verified that the other *s2* accessions carried mutations in both *j2* and *ej2*. PCR genotyping showed all but one accession was double mutant for $ej2^{w}$ and either $j2^{TE}$ or $j2^{stop}$ (Figure S3J). The last accession was homozygous for $ej2^{w}$, but *J2* could not be amplified, consistent with having originated from an X-ray mutagenesis (Stubbe, 1972). Thus, the prolonged meristem maturation underlying *s2* inflorescence branching is caused by mutations in two redundantly acting *SEP* MADS-box genes.

$ej2^{w}$ Arose during Domestication and Hindered *j2* Utilization for Breeding

In modern breeding, the value of jointless varieties was recognized for their potential to reduce fruit drop and post-harvest damage during mechanical harvesting for the processing tomato industry. Yet plants carrying *j1* yield poorly due to reversion of inflorescences to vegetative growth after developing a few flowers (Butler, 1936). Thus, *j2* was widely favored over the last 50 years of breeding. However, breeders frequently experienced problems with excessive inflorescence branching and low yield upon introducing *j2* into different cultivars (Robinson, 1980), probably because of negative epistasis with $ej2^{w}$. To determine to what extent $ej2^{w}$ hindered *j2* utilization in breeding, we genotyped 568 wild and domesticated accessions from our tomato core collection and found that more than half were homozygous for the $ej2^{w}$ allele (Figure 3A and Table S1). Notably, $ej2^{w}$ was absent from *S. pimpinellifolium*, but 40% of early domesticates (landraces) were homozygous for the mutation, and the percentage doubled in cultivars. Importantly, $ej2^{w}$ was strongly associated with long sepals, including within a subset of confirmed landraces (Blanca et al., 2015), suggesting selection during domestication (Figures 3B–3E). In support of this, $ej2^{w}$ is in close proximity (< 46 Kbp) to a previously reported domestication and improvement selective sweep (Lin et al., 2014). Notably, a minor fruit weight QTL (*fw3.2*) that also arose in the landraces is nearby (~85 Kbp) to *EJ2* (Chakrabarti et al., 2013). Among 62 landraces, we found accessions that carried $ej2^{w}$, but not *fw3.2* ($ej2^{w}$/*FW3.2*: 7%), and vice versa (*EJ2*/*fw3.2*: 9%,), suggesting that each allele arose independently and was likely combined early in domestication (Table S1). We also found that not all cultivars carried both alleles ($ej2^{w}$/*FW3.2*: 2%; *EJ2*/*fw3.2*: 11%,), indicating that both mutations were either passed on independently during domestication and improvement or were co-selected and then separated later by breeding (Table S1).

One explanation for the early selection of $ej2^{w}$ and its subsequent spread in the cultivated germplasm is that larger sepals provided an enlarged calyx that was concomitantly selected as fruit size increased, perhaps with *fw3.2*. Such a trait would not necessarily have been selected for improved productivity by increasing fruit size or number per se but instead could have provided improved fruit support, strong local source tissue, or simply aesthetic value for larger fruits. To determine if $ej2^{w}$ was selected during domestication and breeding of larger fruits, we evaluated the frequency of the $ej2^{w}$ allele in 258 cultivars representing five fruit sizes ranging from small "cherry" tomatoes (< 5 g) to extremely large "beefsteak" varieties (> 500 g). Remarkably, the frequency of the allele increased with fruit size, and nearly all (> 90%) large-fruited accessions were homozygous for $ej2^{w}$, including 88% of vintage heirloom cultivars. These results show that the $ej2^{w}$ allele was already widespread in larger fruit types before *j2* was discovered and adopted in modern breeding (Figure 3F and Table S1). Since *EJ2* is also expressed in developing fruits (Figure S4A) and $ej2^{CR}$ fruits are elongated (Figure 2L), it is also possible that the $ej2^{w}$ allele

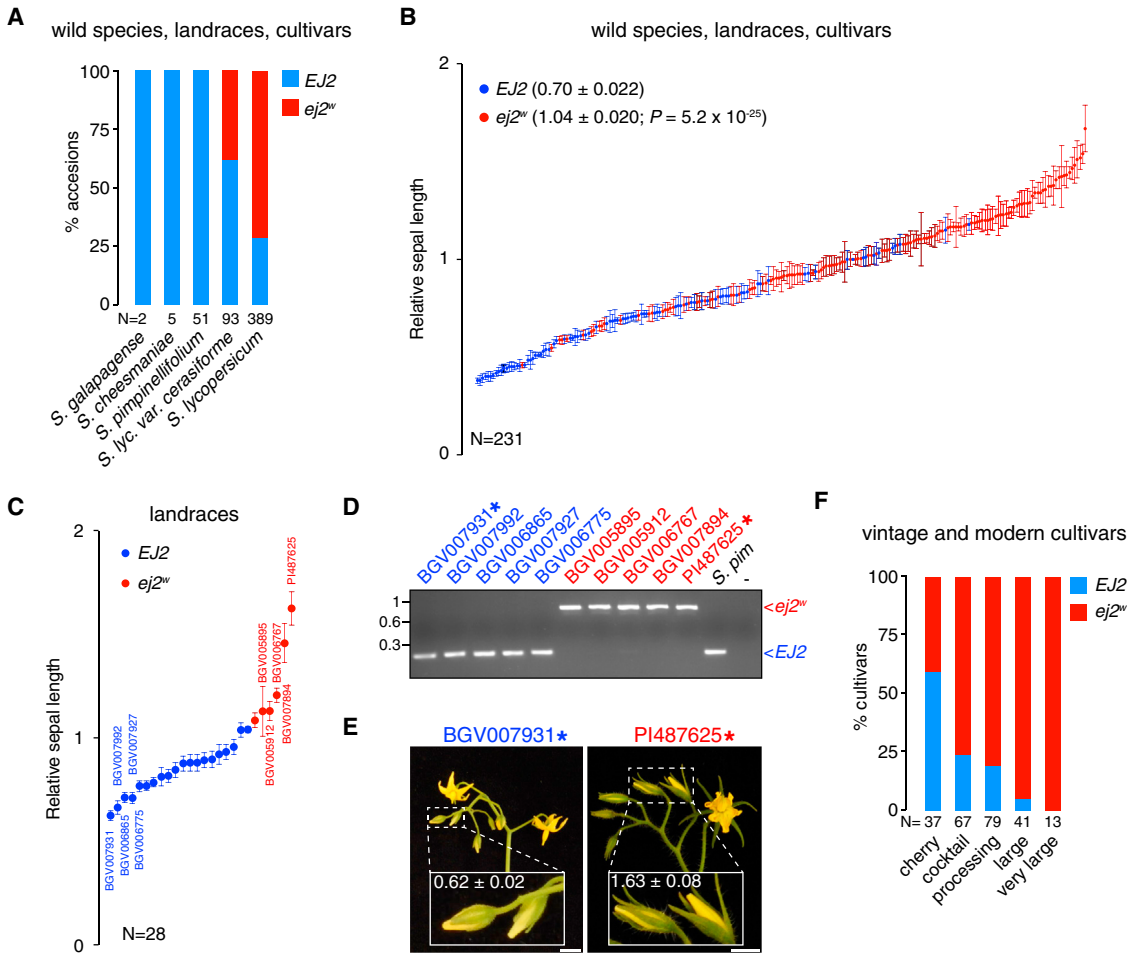

Figure 3. The *ej2*^{w} Variant Arose during Domestication and Was Selected during Breeding of Large-Fruited Cultivars

(A) Distribution of the *ej2*^{w} allele in wild tomato species, early domesticates (landraces, *S. lyc. var. cerasiforme*), and cultivars (*S. lycopersicum*) (N = number of accessions).

(B) Relative sepal length (sepal length/petal length) from a subset of accessions in (A) homozygous for *EJ2* and *ej2*^{w}.

(C) Relative sepal length in a subset of confirmed landraces (Blanca et al., 2015).

(D) PCR genotyping for the *ej2*^{w} allele in 10 landraces with the longest and shortest sepals. *S. pimpinellifolium* (*S. pim*) was used as a WT control.

(E) Inflorescences and flowers (inset) of the accessions with the shortest and longest sepals. See asterisks in (D). Numbers indicate relative sepal length.

(F) PCR genotyping in 258 cultivars shows enrichment of the *ej2*^{w} allele in large-fruited types.

Data in (B), (C), and (E) are means (± SEM, n = 10 flowers per accession). N, number of accessions. *P*, two-tailed, two-sample t test. Scale bars, 1cm.

impacts other fruit traits such as size, shape, or ripening, especially in the presence of other QTL that impact these traits.

Elite Breeding Germplasm Carries Both *j2*^{TE} and *ej2*^{w}, but Branching Is Suppressed

Because *ej2*^{w} became widespread in tomato germplasm and *j2* arose much later, introducing either of the *j2* alleles into most cultivars would have resulted in undesirable branching and low yield. However, it was reported that these adverse effects could be overcome by breeding (Robinson, 1980). One possibility is that *ej2*^{w} was segregated away through crosses. Alternatively, breeders could have identified and selected natural suppressors of branching. To test this, we obtained 153 unbranched jointed and jointless elite inbreds and hybrids from major seed companies and public breeders (see STAR Methods), and we genotyped them for both mutations. All jointless lines were homozygous for *j2*^{TE}, indicating that the allele that arose in the domesticated germplasm was favored in breeding. Since tomato varieties for processing and fresh-market production are developed in separate breeding programs, we asked if *j2*^{TE} was utilized in both. The value of the jointless trait is most recognized for mechanical harvesting of processing types, and in support of this, the *j2*^{TE} allele was present in 74% of sampled processing lines (Table S2). Although less widespread, we also found *j2*^{TE} in 34% of fresh-market lines, indicating that *j2*^{TE} continues to be utilized in both breeding programs.

Unexpectedly, we found that more than 60% of *j2*^{TE} homozygotes in both processing and fresh-market lines were also homozygous for *ej2*^{w} (Figures 4A and 4B), supporting that suppressors were selected during improvement. This reminded us of the

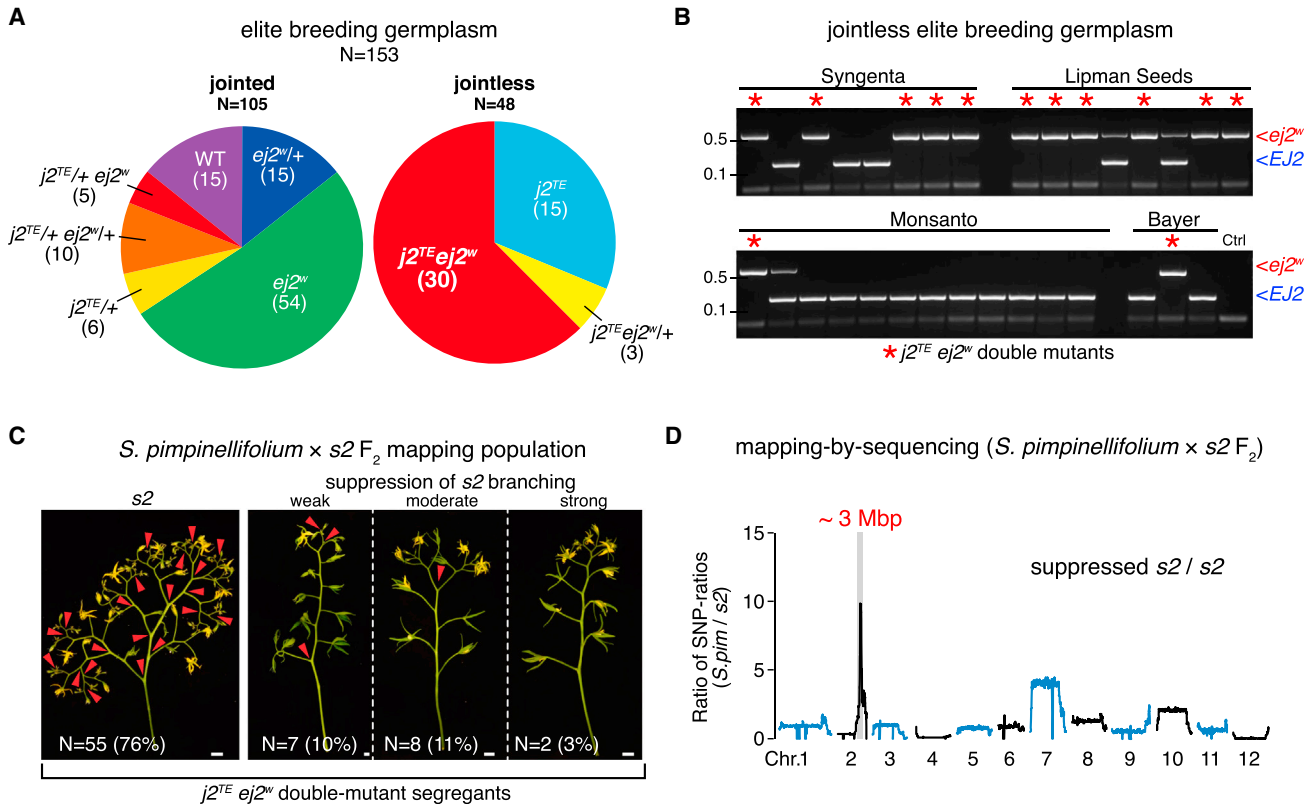

Figure 4. Breeders Overcame Negative Epistasis between *j2* and *ej2* by Selecting Suppressors of *s2* Branching in Elite Germplasm

(A) PCR genotyping of 153 elite breeding lines for $j2^{TE}$ and $ej2^{w}$ reveals that the jointless germplasm is dominated by the *j2* transposon allele and contains many $j2^{TE}$ $ej2^{w}$ double mutants. Number of accessions is indicated in parenthesis.

(B) PCR genotyping of 31 jointless inbreds and hybrids from 4 major seed companies for $ej2^{w}$. Red asterisks indicate $j2^{TE}$ $ej2^{w}$ double mutants.

(C) Representative images of phenotypic classes found in $j2^{TE}$ $ej2^{w}$ double mutants isolated from an *S. pimpinellifolium* × *s2* F_2 population. N indicates number of plants, and percentage of plants in each phenotypic class is indicated in parentheses.

(D) Mapping-by-sequencing a suppressor of *s2* to a 3Mbp interval on chromosome 2 containing 167 genes. DNA from pools of *s2* and suppressed *s2* plants was sequenced, and the ratio (suppressed *s2*/*s2*) of the SNP-ratios (*S.pim*/*s2*) is presented.

See also Table S2 and STAR Methods.

reduced segregation of *s2* in our *S. pimpinellifolium* F_2 mapping population (Figures S3B and S3C). To map potential suppressor loci, we regrew 1,536 F_2 plants, and of 92 plants homozygous for both mutations, 24% showed various degrees of suppression (Figures 4C). Using genome sequencing, we mapped one large-effect suppressor near the end of chromosome 2 in the same region as a previously reported suppressor in the domesticated germplasm (Figures 4D) (Robinson, 1980). However, given that only a small percentage of $j2^{TE}$ $ej2^{w}$ F_2 plants displayed unbranched inflorescences, additional suppressors from breeding germplasm are likely involved, which together were needed to achieve complete suppression.

Three Meristem Expressed *SEP4* Genes Modulate Inflorescence Complexity

The dissection of the negative epistasis underlying *s2* branching exposed two tomato *SEP4* genes that act redundantly to control meristem maturation and inflorescence development. This led us ask to what extent these genes work with other *SEP* family members to regulate inflorescence architecture and flower production and to what extent these genes could have potential for agricultural application. In *Arabidopsis*, a family of four redundant *SEP* genes is required to establish floral organ identity (Ditta et al., 2004; Pelaz et al., 2000). Tomato has an expanded *SEP* family of six members, and a phylogenetic analysis of protein sequences showed that *Arabidopsis* SEP1, 2, and 3 have two tomato homologs (Solyc05g015750/TM5 and Solyc02g089200/TM29) (Figure 5A). In contrast, there are four homologs of *SEP4*, and among them is the *RIPENING INHIBITOR* (*RIN*) gene. A classical mutation in *RIN* blocks ripening and is widely used in hybrid breeding due to a heterozygous dosage effect that causes fruits to remain firm and ripen over a protracted period, improving shelf life (Klee and Giovannoni, 2011; Vrebalov et al., 2002).

To investigate individual and combined roles of tomato *SEP* genes in inflorescence development, we first analyzed expression patterns using our meristem maturation atlas and transcriptome data from other major tissues (Consortium, 2012; Park et al., 2012). Both *TM5* and *TM29* (*SEP1/2/3* homologs) were expressed only later in reproductive development, beginning in

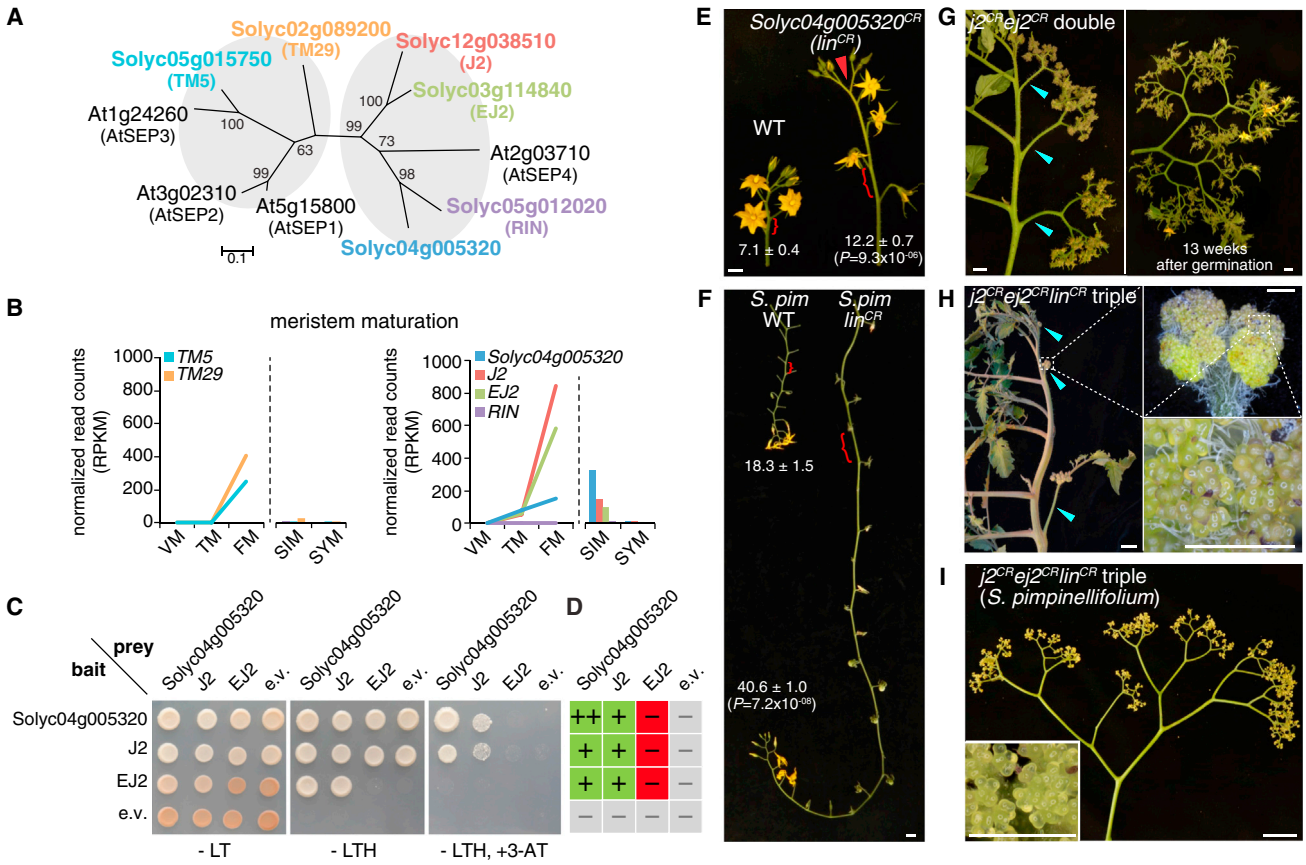

Figure 5. Redundancy among Three *SEP4* Genes Regulates Inflorescence Branching and Flower Development

(A) Phylogenetic tree of SEP proteins in *Arabidopsis* and tomato. Bootstrap values (%) for 1,000 replicates are shown.

(B) Normalized gene expression (RPKM) for *TM5* and *TM29* (left) and the *SEP4* sub-clade (right) during meristem maturation (VM, vegetative meristem; TM, transition meristem; FM, floral meristem; SIM, sympodial inflorescence meristem; SYM, sympodial shoot meristem).

(C) Yeast two-hybrid assays showing heteromeric interactions for Solyc04g005320, J2, and EJ2 and homomeric interactions for Solyc04g005320 and J2 (3-AT, 3-amino-1,2,4-triazole; L, leucine; T, tryptophan; H, histidine; e.v., empty vector).

(D) Summary of results in (C); −, no interaction; +, interaction; ++, strong interaction.

(E) Longer inflorescence of a *Solyc04g005320*^{CR} mutant (hereafter referred to as *long inflorescence*^{CR}; *lin*^{CR}) compared to WT. Numbers indicate flowers per inflorescence (mean ± SEM, N = 10 inflorescences). *P* two-tailed, two-sample t test. Scale bar, 1 cm.

(F) Longer inflorescence of a *Solyc04g005320*^{CR} mutant in *S. pimpinellifolium* (*S. pim lin*^{CR}) compared to *S. pimpinellifolium* WT.

(G) *j2*^{CR} *ej2*^{CR} double mutant plant (left) and inflorescence (right) showing SIM overproliferation and few flowers late in development, respectively.

(H) *j2*^{CR} *ej2*^{CR} *lin*^{CR} triple mutant. Stereoscope images (insets) of *j2*^{CR} *ej2*^{CR} *lin*^{CR} triple mutants showing massive SIM overproliferation and no floral termination.

(I) *j2*^{CR} *ej2*^{CR} *lin*^{CR} triple mutant in *S. pimpinellifolium* as in (H), showing massive SIM overproliferation and no floral termination.

Cyan arrowheads indicate successive inflorescences. Scale bars represent 1 cm and 1 mm for photographs and stereoscopic images, respectively.

See also Figure S4 and STAR Methods.

floral meristems and extending into flowers and fruits (Figures 5B and S4A), supporting previously characterized roles in floral organ identity (Ampomah-Dwamena et al., 2002; Pnueli et al., 1994). *RIN* was only expressed in fruits, consistent with its role in ripening (Figure S4A)(Vrebalov et al., 2002). In contrast, expression of *J2*, *EJ2*, and the fourth *SEP4* homolog (*Solyc04g005320*) began earlier, in the TM stage of meristem maturation and in SIMs (Figure 5B). This suggested that *Solyc04g005320* functions with *J2* and *EJ2* in meristem maturation. Moreover, given that *Arabidopsis SEP* redundancy is based on formation of multimeric protein complexes (Theißen et al., 2016), we tested interactions among all four tomato SEP4 proteins in yeast two-hybrid assays and found that J2, EJ2, and Solyc04g005320 interacted with each other and themselves, except for homomeric EJ2. These results validated previous findings (Leseberg et al., 2008) and further revealed that J2 and EJ2 interact with each other, supporting redundancy in the control of meristem maturation and inflorescence architecture (Figures 5C, 5D, S4B, and S4C).

To test if *Solyc04g005320* contributes to inflorescence architecture and flower production, we used CRISPR/Cas9 to engineer plants with null mutations, which resulted in exceptionally long inflorescences with nearly twice as many flowers as WT and longer internodes (Figures 5E and S4D). We also frequently observed weak branching late in inflorescence development. We tested if similar effects occur in genotypes that already have long

inflorescences by mutating *Solyc04g005320* in *S. pimpinellifolium,* which produces 15–20 flowers on each inflorescence. Remarkably, internode length and flower number doubled (Figures 5F, and S4D–S4F). These phenotypes reminded us of a gamma-irradiation mutant that we designated *long inflorescence* (*lin*) and previously mapped to an interval on chromosome 4 containing *Solyc04g005320* (Figures S4G–S4J) (see STAR Methods). Sequencing *Solyc04g005320* from the *lin* mutant revealed a translocation in the first intron that eliminated transcription (Figures S4J–S4L), and crosses with a CRISPR allele failed to complement the long inflorescence phenotype.

The increase in inflorescence complexity in *lin* mutants is modest compared to *j2 ej2*^{w} double mutants. To study the extent of redundancy and potential dosage relationships among the three genes, we used strong alleles in the same background to create all combinations of higher-order mutants (see STAR Methods). Whereas *j2*^{CR} was largely additive with *lin* (Figure S4M), *ej2*^{CR} and *lin* were synergistic for floral organ development; double mutants had long inflorescences with more flowers that developed extremely enlarged sepals, but inner floral organs did not fully develop, and fruits failed to form (Figure S4N). As expected, *j2*^{CR} and *ej2*^{CR} were also synergistic, but unlike the moderately branched, highly floral inflorescences of the original *j2*$^{TE/stop}$ *ej2*^{w} natural double mutants (*s2*), inflorescences from *j2*^{CR} *ej2*^{CR} plants were extraordinarily branched and rarely produced normal fertile flowers (Figure 5G). Finally, combining all three mutants resulted in massively overproliferated SIMs without forming flowers (Figures 5H and S4O). We observed the same effect in *S. pimpinellifolium j2*^{CR} *ej2*^{CR} *lin*^{CR} plants (Figures 5I and S4O). Thus, *J2* and *EJ2* have distinct roles in floral development, but all three *SEP4* genes have overlapping roles in meristem maturation and inflorescence development.

Dosage of Meristem Maturation Transcription Factors Can Be Exploited to Improve Inflorescence Architecture and Yield

The individual and combined mutations in *J2*, *EJ2*, and *LIN* provide a series of increased inflorescence complexity ranging from weak (*lin* single mutants) to extremely severe (*j2 ej2 lin* triple mutants), indicating quantitative relationships among these *SEP4* genes. We previously demonstrated that dosage relationships among genes in the florigen pathway could be exploited to create a quantitative range of plant architectures that translated to improved productivity in determinate field-grown tomatoes (Park et al., 2014b; Soyk et al., 2017). We reasoned that dosage sensitivity could be similarly used to fine-tune inflorescence architecture and flower production. To test this, we first created a series of homozygous and heterozygous combinations of *j2* strong alleles with *ej2*^{w} or *ej2*^{CR} in the isogenic M82 background (Figures 6A and 6B). All double heterozygotes (e.g., *j2*/+ *ej2*^{w}/+; *j2*/+ *ej2*^{CR}/+) and plants heterozygous for *j2* and homozygous for *ej2*^{w} (*j2*/+ *ej2*^{w}) produced unbranched inflorescences like the single mutants. In contrast, heterozygosity for *ej2*^{w} in a *j2* background (*j2 ej2*^{w}/+) conferred weak branching, as did *j2*/+ *ej2*^{CR}. Notably, heterozygosity for the null *ej2*^{CR} allele in the null *j2* background (*j2 ej2*^{CR}/+) resulted in branching that matched *s2* inflorescences (*j2 ej2*^{w}), further validating that *ej2*^{w} is a weak allele and confirming a sensitive dosage relationship between these genes. Given these results, we reasoned that other meristem maturation regulators might have similar dosage sensitivity on inflorescence architecture and tested this with *S*, a member of the WOX protein family (Lippman et al., 2008). Indeed, plants heterozygous for three *s* mutant alleles were also mildly branched (Figures 6C and 6D), demonstrating that dosage sensitivity of independent meristem maturation genes allows for quantitative tuning of inflorescence architecture.

To evaluate the agronomic potential of weakly branched genotypes for improving flower production and yield, we selected lines from a cherry fresh-market tomato-breeding program that segregated *j2*^{TE}, *ej2*^{w}, and *s* mutants (Figure 6E and STAR Methods). We used this germplasm to test for improved productivity in the context of protected indoor cultivation (greenhouses), which is dominated by indeterminate hybrid varieties that continuously produce new shoots and inflorescences from sympodial shoot meristems (SYMs) over long growing seasons (~9 months) (Park et al., 2014a; Peet and Welles, 2005). Importantly, in greenhouse production, each plant is pruned to maintain one or two main shoots. Yield therefore depends on a limited number of inflorescences, making improved inflorescence architecture and fruit set an important target to increase yield.

By crossing two different *s2* cherry F_3 inbred (*j2*^{TE} *ej2*^{w}) lines with a jointless plum F_6 inbred (*j2*^{TE}) (see STAR Methods), new hybrid lines were produced. These two pre-breeding experiments served to evaluate the potential of heterozygosity for *ej2*^{w} to improve inflorescence architecture and fruit yield in a jointless background. Both *j2*^{TE} *ej2*^{w}/+ hybrid lines produced inflorescences with more branches and flowers compared to *j2*^{TE} control hybrids (Figures 6F–6I). Notably, total fruit number and yield of *j2*^{TE} *ej2*^{w}/+ hybrids increased by 19%–39% and 41%–71%, respectively, while individual fruit weight increased by 19%–22%, and sugar content (Brix) remained unchanged (Figures 6J–6L and Table S3), indicating that yield gains were mainly driven by more fruits. The *s*/+ hybrids showed an even greater improvement of flower and fruit production and higher yields than *j2*^{TE} *ej2*^{w}/+ hybrid lines (Figures 6M–6S). While further refinements will be needed, these results show that mutant alleles of the three genes, through their dosage effects on meristem maturation, have significant potential for developing weakly branched breeding lines with improved tomato yield.

DISCUSSION

Dose-Dependent Quantitative Variation, Weak Alleles, and Crop Improvement

This study was motivated by our interest in the genetic and molecular control of inflorescence architecture in tomato and in exploring the potential of genes and alleles underlying natural variation in inflorescence complexity to improve productivity. By analyzing the *s2* branching variant, we found that multiple members of the *SEP4* subfamily of tomato MADS-box genes play critical redundant roles in modulating meristem maturation and inflorescence architecture. We further describe the first MADS-box family member involved in tomato domestication, highlighting the growing significance of this transcription factor family in contributing to domestication and improvement of

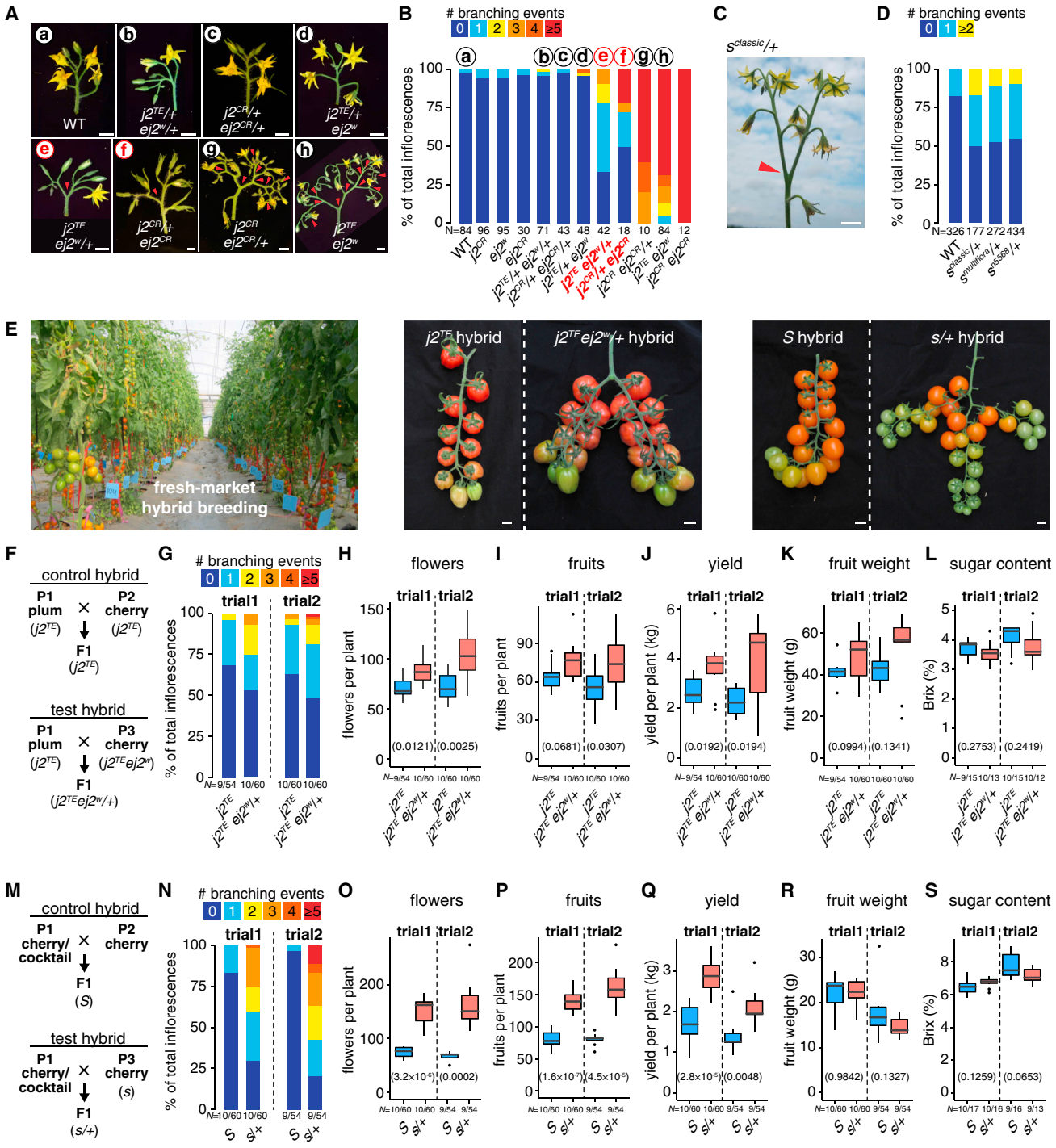

Figure 6. Exploiting Dosage Effects of Key Meristem Maturation Genes to Improve Flower Production and Fruit Yield

(A) Representative inflorescences from natural and engineered *j2* and *ej2* mutant combinations. Red arrowheads indicate branching events.

(B) Percentage of inflorescences with 1–5 or more branching events for the indicated genotypes. Circled, lower-case letters match genotypes shown in (A). Weakly branched genotypes are highlighted in red font.

(C) Representative weakly branched inflorescence of a $s^{classic}$/+ heterozygote.

(D) Percentage of inflorescences with branching events for $s^{classic}$/+, $s^{multiflora}$/+, and s^{n5568}/+ heterozygotes.

(E) An indeterminate fresh-market hybrid productivity trial (left) testing benefits of weakly branched $j2^{TE}$ $ej2^{w}$/+ hybrids (middle) and s/+ hybrids (right) compared to control hybrids.

(legend continued on next page)

diverse crops (Singh et al., 2013; Vrebalov et al., 2002; Zhao et al., 2011). By dissecting interactions between meristem-expressed *SEP4* genes, we uncovered dosage relationships among an allelic series of natural and induced MADS-box mutations with potential for breeding. This collection of alleles, including mutations in *S*, comprises a toolkit to manipulate inflorescence architecture, which can now be expanded to additional regulators of meristem maturation, such as *LIN*. To demonstrate this, we used CRISPR/Cas9 to target *LIN* in the elite cherry tomato cultivar Sweet 100 and generated mutant lines with moderately branched inflorescences and increased flower production (Figure S4P–S).

Our approach for creating desirable phenotypic variation in major yield traits relies on combining specific heterozygous and homozygous mutations to obtain a quantitative range of dosage effects (Park et al., 2014b). However, exploiting gene dosage is limited by the availability of weak alleles that confer quantitative trait modifications. For example, longer sepals and weak branching were achieved through different levels of reduced *EJ2* dosage from homozygosity and heterozygosity for $ej2^{w}$, respectively. In nature, similar dosage effects often arise from mutations in transcriptional control regions (i.e., *cis*-regulatory DNA). Such alleles were widely favored in crop domestication and improvement for their subtle phenotypic changes compared to null alleles that frequently display deleterious pleiotropic effects (Meyer and Purugganan, 2013). For example, increased fruit size during tomato domestication depended in part on transcriptional alleles of multiple components in the classical *CLAVATA-WUSCHEL* stem cell circuit (Xu et al., 2015). A potentially powerful approach to engineer novel weak alleles that we and others are exploring (Swinnen et al., 2016) is exploiting gene-editing technology to mutate *cis*-regulatory control regions of productivity genes. A promising target identified in this study is *LIN*. CRISPR/Cas9-induced weak transcriptional alleles that confer reduced *LIN* expression could provide subtle increases in flower production, which would be especially valuable in large-fruited cultivars, where branching often negatively impacts fruit weight and yield. Notably, a rice homolog of *LIN* and other meristem maturation genes control panicle architecture and grain production (Kobayashi et al., 2010; Liu et al., 2013), suggesting that our findings have broad agricultural potential. New gene-editing tools should enable the engineering of diverse types and strengths of alleles that can provide customized gene dosage effects to improve a wide range of agronomic traits in many crops.

Epistasis in Evolution, Domestication, and Breeding

Progress in breeding is largely driven by loci with predictable additive effects. For example, the majority of flowering time variation in maize is determined by thousands of small additive quantitative trait loci (QTL) (Buckler et al., 2009), and the same is true for traits in other crops (Doust et al., 2014; Gao et al., 2015). Yet epistatic interactions, both positive and negative, are also important in breeding, particularly when working with disparate germplasm. For example, interactions between interspecific QTL in rice can improve aluminum tolerance (Famoso et al., 2011), whereas stacking multiple wild-species-derived QTL affecting the same yield traits in tomato results in less-than-additive or "diminishing returns" epistasis (Eshed and Zamir, 1996).

In recent years, several cases of negative epistasis have emerged in diverse organisms involving clashes between newly evolved and established alleles or upon bringing together distinct genomes, either through natural or artificial means. Examples include compromised fitness gains upon combining interacting alleles in bacteria and yeast (Chou et al., 2011; Heck et al., 2006; Khan et al., 2011; Kvitek and Sherlock, 2011), hybrid necrosis between distinct accessions of *Arabidopsis* (Chae et al., 2014), and loss of protection from malaria in humans when two common resistance variants are co-inherited (Williams et al., 2005). Compared to negative epistasis in evolution and natural selection, the intense artificial selection imposed by humans during domestication and breeding could drive more frequent occurrences of epistasis. While dramatic cases like the one described in this study could be overcome through selection against interactions or suppression with modifiers, there are likely many undiscovered negative interactions in agriculture with more subtle phenotypic consequences that will remain challenging to detect and dissect until high-throughput quantitative phenotyping platforms (phenomics) and power in genome-wide association studies (GWAS) improve.

Our dissection of the extreme negative epistasis underlying the *s2* branching syndrome has highlighted an underappreciated challenge for the next generation of crop breeding. Specifically, using rapidly advancing gene-editing technologies to introduce precise novel allelic variation for specific genes into existing germplasm may not provide desirable phenotypic outcomes and could potentially result in negative consequences due to interactions with alleles selected and stabilized during domestication and early breeding (Mackay, 2014). That our example of negative epistasis involved two closely related MADS-box genes

(F) Crossing scheme for the $j2^{TE}$ $ej2^{w}$/+ hybrid productivity trials. Parental inbreds (e.g., P1) are indicated for each hybrid cross, and genotypes are in parentheses. Female and male parents were plum and cherry varieties, respectively, resulting in hybrids with cocktail-sized fruits.

(G) Percentage of inflorescences with 1–5 or more branching events for $j2^{TE}$ $ej2^{w}$/+ hybrids and $j2^{TE}$ control hybrids. Results for two trials resulting from crossing independent parents of the same genotypes are shown.

(H–L) Flower number (H), fruit number (I), and fruit yield (J) per plant, and average fruit weight (K) and sugar content (L) for the indicated genotypes in the hybrids in (F).

(M) Crossing scheme for generating control and test hybrids for the *s*/+ productivity trials, as in (F).

(N) Percentage of branched inflorescences for control and *s*/+ hybrids, as in (G).

(O–S) Flower number (O), fruit number (P), and fruit yield (Q) per plant, and average fruit weight (R) and sugar content (S) for the indicated genotypes in the hybrids in (M).

Red arrowheads in (A) and (C) mark inflorescence branch points. *N* indicates number of inflorescences (B, D) and number of plants and inflorescences (G–L, N–S). Numbers in parentheses in (H)–(L) and (O)–(S) represent *P* values (two-tailed, two-sample t test). Scale bars in (A), (C), and (E) indicate 1 cm.

See also Table S3 and STAR Methods.

suggests that engineering new alleles in gene families or related developmental pathways that already played a role in domestication and improvement would be particularly sensitive to unexpected epistatic consequences, perhaps explaining other as-yet-uncharacterized examples of negative epistasis in agriculture (Bomblies and Weigel, 2007; Matsubara et al., 2015; Shang et al., 2016; Zhang et al., 2011). Elucidating, neutralizing, and potentially exploiting negative epistasis could have a significant impact in helping break productivity barriers in breeding of both plants and animals.

STAR★METHODS

Detailed methods are provided in the online version of this paper and include the following:

- KEY RESOURCES TABLE
- CONTACT FOR REAGENT AND RESOURCE SHARING
- EXPERIMENTAL MODEL AND SUBJECT DETAILS
  - Plant material and growth conditions
- METHOD DETAILS
  - Plant phenotyping
  - Yeast two-hybrid analysis
  - Meristem imaging
  - Meristem transcriptome profiling
  - Mapping-by-sequencing
  - Tissue collection and RNA extraction
  - Phylogenetic analyses and sequence analyses
  - CRISPR/Cas9 mutagenesis, plant transformation, and selection of mutant alleles
  - Generation of parental and hybrid lines for cherry tomato breeding and yield trials under agricultural greenhouse conditions
- QUANTIFICATION AND STATISTICAL ANALYSES
  - Sampling
  - Transcriptome quantification
  - Mapping
- DATA AND SOFTWARE AVAILABILITY
- ADDITIONAL RESOURCES

SUPPLEMENTAL INFORMATION

Supplemental Information includes four figures and four tables and can be found with this article online at http://dx.doi.org/10.1016/j.cell.2017.04.032.

A video abstract is available at http://dx.doi.org/10.1016/j.cell.2017.04.032#mmc5.

AUTHOR CONTRIBUTIONS

S.S., Z.H.L., S.J.P., A.G., K.J., E.v.d.K., J.V.E., D.Z., Y.E., and Z.B.L. designed and planned experiments. S.S., Z.H.L., M.O., J.F., K.L.L., S.J.P., A.G., K.J., A.R., E.v.d.K., and Z.B.L. performed experiments and collected the data. S.S., Z.H.L., M.O., J.F., S.J.P., K.J., and Z.B.L. analyzed the data. S.S., Z.H.L., D.Z., Y.E., and Z.B.L. designed the research. S.S., Z.H.L., and Z.B.L. wrote the paper with input from all other authors.

ACKNOWLEDGMENTS

We thank all members of the Lippman lab for valuable discussions. We thank C. Brooks, A. Krainer, and J. Dalrymple for technical support, P. Keen for assistance with tomato transformation, T. Mulligan, S. Vermylen, and S. Qiao from CSHL, and staff from Cornell University's Long Island Horticultural Research and Extension Center for assistance with plant care. We thank I. Zemach for assistance with constructing populations for hybrid breeding and help with data collection. We thank J. Bonnet (Syngenta), M. Barineau (Lipman Seeds), D. Drost and C. Braun (Monsanto), F. Millenaar and I. Stein (Bayer Crop Science), S. Hutton (University of Florida), and T. Ariizumi (University of Tsukuba) for providing seed, tissue, and DNA samples. This research was supported by an EMBO Long-Term Fellowship (ALTF 1589-2014) to S.S., a National Science Foundation Postdoctoral Research Fellowship in Biology Grant (IOS-1523423) to Z.H.L., the Next-Generation BioGreen 21 Program (SSAC, PJ01188301) to S.J.P., the National Science Foundation Plant Genome Research Program (IOS-1564366) to E.v.d.K., a European Research Council - Advanced Grant entitled YIELD (ERC-294691) to D.Z., the US-Israel Binational Agricultural Research & Development fund (BARD, IS-4818-15) to Z.B.L. and Y.E., and the National Science Foundation Plant Genome Research Program (IOS-1237880) to J.V.E. and Z.B.L.

Received: March 10, 2017
Revised: April 13, 2017
Accepted: April 24, 2017
Published: May 18, 2017

REFERENCES

Ampomah-Dwamena, C., Morris, B.A., Sutherland, P., Veit, B., and Yao, J.L. (2002). Down-regulation of TM29, a tomato SEPALLATA homolog, causes parthenocarpic fruit development and floral reversion. Plant Physiol. *130*, 605–617.

Anders, S., Pyl, P.T., and Huber, W. (2015). HTSeq–a Python framework to work with high-throughput sequencing data. Bioinformatics *31*, 166–169.

Belhaj, K., Chaparro-Garcia, A., Kamoun, S., and Nekrasov, V. (2013). Plant genome editing made easy: targeted mutagenesis in model and crop plants using the CRISPR/Cas system. Plant Methods *9*, 39.

Bemer, M., Karlova, R., Ballester, A.R., Tikunov, Y.M., Bovy, A.G., Wolters-Arts, M., Rossetto, P.d.B., Angenent, G.C., and de Maagd, R.A. (2012). The tomato FRUITFULL homologs TDR4/FUL1 and MBP7/FUL2 regulate ethylene-independent aspects of fruit ripening. Plant Cell *24*, 4437–4451.

Blanca, J., Montero-Pau, J., Sauvage, C., Bauchet, G., Illa, E., Díez, M.J., Francis, D., Causse, M., van der Knaap, E., and Cañizares, J. (2015). Genomic variation in tomato, from wild ancestors to contemporary breeding accessions. BMC Genomics *16*, 257.

Boden, S.A., Cavanagh, C., Cullis, B.R., Ramm, K., Greenwood, J., Jean Finnegan, E., Trevaskis, B., and Swain, S.M. (2015). Ppd-1 is a key regulator of inflorescence architecture and paired spikelet development in wheat. Nat. Plants *1*, 14016.

Bolger, A., Scossa, F., Bolger, M.E., Lanz, C., Maumus, F., Tohge, T., Quesneville, H., Alseekh, S., Sørensen, I., Lichtenstein, G., et al. (2014a). The genome of the stress-tolerant wild tomato species Solanum pennellii. Nat. Genet. *46*, 1034–1038.

Bolger, A.M., Lohse, M., and Usadel, B. (2014b). Trimmomatic: a flexible trimmer for Illumina sequence data. Bioinformatics *30*, 2114–2120.

Bomblies, K., and Weigel, D. (2007). Hybrid necrosis: autoimmunity as a potential gene-flow barrier in plant species. Nat. Rev. Genet. *8*, 382–393.

Brooks, C., Nekrasov, V., Lippman, Z.B., and Van Eck, J. (2014). Efficient gene editing in tomato in the first generation using the clustered regularly interspaced short palindromic repeats/CRISPR-associated9 system. Plant Physiol. *166*, 1292–1297.

Buckler, E.S., Holland, J.B., Bradbury, P.J., Acharya, C.B., Brown, P.J., Browne, C., Ersoz, E., Flint-Garcia, S., Garcia, A., Glaubitz, J.C., et al. (2009). The genetic architecture of maize flowering time. Science *325*, 714–718.

Budiman, M.A., Chang, S.B., Lee, S., Yang, T.J., Zhang, H.B., de Jong, H., and Wing, R.A. (2004). Localization of jointless-2 gene in the centromeric region of

tomato chromosome 12 based on high resolution genetic and physical mapping. Theor. Appl. Genet. *108*, 190–196.

Butler, L. (1936). Inherited characters in the tomato. II. Jointless pedicels. J. Hered. *27*, 25–26.

Chae, E., Bomblies, K., Kim, S.T., Karelina, D., Zaidem, M., Ossowski, S., Martín-Pizarro, C., Laitinen, R.A.E., Rowan, B.A., Tenenboim, H., et al. (2014). Species-wide genetic incompatibility analysis identifies immune genes as hot spots of deleterious epistasis. Cell *159*, 1341–1351.

Chakrabarti, M., Zhang, N., Sauvage, C., Muños, S., Blanca, J., Cañizares, J., Diez, M.J., Schneider, R., Mazourek, M., McClead, J., et al. (2013). A cytochrome P450 regulates a domestication trait in cultivated tomato. Proc. Natl. Acad. Sci. USA *110*, 17125–17130.

Chou, H.-H., Chiu, H.-C., Delaney, N.F., Segrè, D., and Marx, C.J. (2011). Diminishing returns epistasis among beneficial mutations decelerates adaptation. Science *332*, 1190–1192.

Consortium, T.T.G.; Tomato Genome Consortium (2012). The tomato genome sequence provides insights into fleshy fruit evolution. Nature *485*, 635–641.

Ditta, G., Pinyopich, A., Robles, P., Pelaz, S., and Yanofsky, M.F. (2004). The SEP4 gene of Arabidopsis thaliana functions in floral organ and meristem identity. Curr. Biol. *14*, 1935–1940.

Doebley, J., Stec, A., and Hubbard, L. (1997). The evolution of apical dominance in maize. Nature *386*, 485–488.

Doust, A.N., Lukens, L., Olsen, K.M., Mauro-Herrera, M., Meyer, A., and Rogers, K. (2014). Beyond the single gene: How epistasis and gene-by-environment effects influence crop domestication. Proc. Natl. Acad. Sci. USA *111*, 6178–6183.

Eshed, Y., and Zamir, D. (1996). Less-than-additive epistatic interactions of quantitative trait loci in tomato. Genetics *143*, 1807–1817.

Famoso, A.N., Zhao, K., Clark, R.T., Tung, C.W., Wright, M.H., Bustamante, C., Kochian, L.V., and McCouch, S.R. (2011). Genetic architecture of aluminum tolerance in rice (Oryza sativa) determined through genome-wide association analysis and QTL mapping. PLoS Genet. *7*, e1002221.

Futschik, M. (2015). Mfuzz: Soft clustering of time series gene expression data. R package version 2.30.0. http://www.sysbiolab.eu/software/R/Mfuzz/index.html.

Gao, X., Zhang, X., Lan, H., Huang, J., Wang, J., and Zhang, H. (2015). The additive effects of GS3 and qGL3 on rice grain length regulation revealed by genetic and transcriptome comparisons. BMC Plant Biol. *15*, 156.

Gupta, S., and Van Eck, J. (2016). Modification of plant regeneration medium decreases the time for recovery of Solanum lycopersicum cultivar M82 stable transgenic lines. Plant Cell Tiss. Organ Cult. *127*, 417–423.

Heck, J.A., Argueso, J.L., Gemici, Z., Reeves, R.G., Bernard, A., Aquadro, C.F., and Alani, E. (2006). Negative epistasis between natural variants of the Saccharomyces cerevisiae MLH1 and PMS1 genes results in a defect in mismatch repair. Proc. Natl. Acad. Sci. USA *103*, 3256–3261.

Huang, X., Qian, Q., Liu, Z., Sun, H., He, S., Luo, D., Xia, G., Chu, C., Li, J., and Fu, X. (2009). Natural variation at the DEP1 locus enhances grain yield in rice. Nat. Genet. *41*, 494–497.

Khan, A.I., Dinh, D.M., Schneider, D., Lenski, R.E., and Cooper, T.F. (2011). Negative epistasis between beneficial mutations in an evolving bacterial population. Science *332*, 1193–1196.

Kim, D., Pertea, G., Trapnell, C., Pimentel, H., Kelley, R., and Salzberg, S.L. (2013). TopHat2: accurate alignment of transcriptomes in the presence of insertions, deletions and gene fusions. Genome Biol. *14*, R36.

Klee, H.J., and Giovannoni, J.J. (2011). Genetics and control of tomato fruit ripening and quality attributes. Annu. Rev. Genet. *45*, 41–59.

Kobayashi, K., Maekawa, M., Miyao, A., Hirochika, H., and Kyozuka, J. (2010). PANICLE PHYTOMER2 (PAP2), encoding a SEPALLATA subfamily MADS-box protein, positively controls spikelet meristem identity in rice. Plant Cell Physiol. *51*, 47–57.

Kvitek, D.J., and Sherlock, G. (2011). Reciprocal sign epistasis between frequently experimentally evolved adaptive mutations causes a rugged fitness landscape. PLoS Genet. *7*, e1002056.

Kyozuka, J., Tokunaga, H., and Yoshida, A. (2014). Control of grass inflorescence form by the fine-tuning of meristem phase change. Curr. Opin. Plant Biol. *17*, 110–115.

Lei, Y., Lu, L., Liu, H.Y., Li, S., Xing, F., and Chen, L.L. (2014). CRISPR-P: a web tool for synthetic single-guide RNA design of CRISPR-system in plants. Mol. Plant *7*, 1494–1496.

Lemmon, Z.H., Park, S.J., Jiang, K., Van Eck, J., Schatz, M.C., and Lippman, Z.B. (2016). The evolution of inflorescence diversity in the nightshades and heterochrony during meristem maturation. Genome Res. *26*, 1676–1686.

Leseberg, C.H., Eissler, C.L., Wang, X., Johns, M.A., Duvall, M.R., and Mao, L. (2008). Interaction study of MADS-domain proteins in tomato. J. Exp. Bot. *59*, 2253–2265.

Li, H. (2011). A statistical framework for SNP calling, mutation discovery, association mapping and population genetical parameter estimation from sequencing data. Bioinformatics *27*, 2987–2993.

Li, H. (2013). Aligning sequence reads, clone sequences and assembly contigs with BWA-MEM. arXiv Prepr. arXiv *0*, 3.

Li, H., and Durbin, R. (2009). Fast and accurate short read alignment with Burrows-Wheeler transform. Bioinformatics *25*, 1754–1760.

Li, H., Handsaker, B., Wysoker, A., Fennell, T., Ruan, J., Homer, N., Marth, G., Abecasis, G., and Durbin, R.; 1000 Genome Project Data Processing Subgroup (2009). The Sequence Alignment/Map format and SAMtools. Bioinformatics *25*, 2078–2079.

Lin, T., Zhu, G., Zhang, J., Xu, X., Yu, Q., Zheng, Z., Zhang, Z., Lun, Y., Li, S., Wang, X., et al. (2014). Genomic analyses provide insights into the history of tomato breeding. Nat. Genet. *46*, 1220–1226.

Lippman, Z.B., Cohen, O., Alvarez, J.P., Abu-Abied, M., Pekker, I., Paran, I., Eshed, Y., and Zamir, D. (2008). The making of a compound inflorescence in tomato and related nightshades. PLoS Biol. *6*, e288.

Liu, C., Teo, Z.W.N., Bi, Y., Song, S., Xi, W., Yang, X., Yin, Z., and Yu, H. (2013). A conserved genetic pathway determines inflorescence architecture in Arabidopsis and rice. Dev. Cell *24*, 612–622.

Liu, D., Wang, D., Qin, Z., Zhang, D., Yin, L., Wu, L., Colasanti, J., Li, A., and Mao, L. (2014). The SEPALLATA MADS-box protein SLMBP21 forms protein complexes with JOINTLESS and MACROCALYX as a transcription activator for development of the tomato flower abscission zone. Plant J. *77*, 284–296.

Macarthur, J.W., and Chiasson, L.P. (1947). Cytogenetic Notes on Tomato Species and Hybrids. Genetics *32*, 165–177.

Mackay, T.F.C. (2014). Epistasis and quantitative traits: using model organisms to study gene-gene interactions. Nat. Rev. Genet. *15*, 22–33.

Mao, L., Begum, D., Chuang, H.W., Budiman, M.A., Szymkowiak, E.J., Irish, E.E., and Wing, R.A. (2000). JOINTLESS is a MADS-box gene controlling tomato flower abscission zone development. Nature *406*, 910–913.

Matsubara, K., Yamamoto, E., Mizobuchi, R., Yonemaru, J., Yamamoto, T., Kato, H., and Yano, M. (2015). Hybrid breakdown caused by epistasis-based recessive incompatibility in a cross of rice (Oryza sativa L.). J. Hered. *106*, 113–122.

Meyer, R.S., and Purugganan, M.D. (2013). Evolution of crop species: genetics of domestication and diversification. Nat. Rev. Genet. *14*, 840–852.

Mullins, M.G., Bouquet, A., and Williams, L.E. (1992). Biology of the Grapevine (Cambridge Univ. Press).

Nakano, T., Kimbara, J., Fujisawa, M., Kitagawa, M., Ihashi, N., Maeda, H., Kasumi, T., and Ito, Y. (2012). MACROCALYX and JOINTLESS interact in the transcriptional regulation of tomato fruit abscission zone development. Plant Physiol. *158*, 439–450.

Park, S.J., Jiang, K., Schatz, M.C., and Lippman, Z.B. (2012). Rate of meristem maturation determines inflorescence architecture in tomato. Proc. Natl. Acad. Sci. USA *109*, 639–644.

Park, S.J., Eshed, Y., and Lippman, Z.B. (2014a). Meristem maturation and inflorescence architecture–lessons from the Solanaceae. Curr. Opin. Plant Biol. *17*, 70–77.

Park, S.J., Jiang, K., Tal, L., Yichie, Y., Gar, O., Zamir, D., Eshed, Y., and Lippman, Z.B. (2014b). Optimization of crop productivity in tomato using induced mutations in the florigen pathway. Nat. Genet. *46*, 1337–1342.

Peet, M.M., and Welles, G. (2005). Greenhouse tomato production, N. Tomatoes and E. Heuvelink, eds. (Wallingford: U.K. CABI Publ.), pp. 257–304.

Pelaz, S., Ditta, G.S., and Yanofsky, M.F. (2000). B and C foral organ identity functions require SEPALLATA MADS-box genes. Nature *405*, 200–203.

Peralta, I.E., and Spooner, D.M. (2005). Morphological Characterization and Relationships of Wild Tomatoes (*Solanum L.* Section *Lycopersicon*). Missouri Botanical Garden Press. *104*, 227–257.

Pnueli, L., Hareven, D., Broday, L., Hurwitz, C., and Lifschitz, E. (1994). The TM5 MADS Box Gene Mediates Organ Differentiation in the Three Inner Whorls of Tomato Flowers. Plant Cell *6*, 175–186.

Ramsay, L., Comadran, J., Druka, A., Marshall, D.F., Thomas, W.T.B., Macaulay, M., MacKenzie, K., Simpson, C., Fuller, J., Bonar, N., et al. (2011). INTERMEDIUM-C, a modifier of lateral spikelet fertility in barley, is an ortholog of the maize domestication gene TEOSINTE BRANCHED 1. Nat. Genet. *43*, 169–172.

Reynard, G.B. (1961). New Source of the j2 Gene Governing Jointless Pedicel in Tomato. Science *134*, 2102.

Rick, C.M. (1956a). Genetic and Systematic Studies on Accessions of Lycospersicon from the Galapagos Islands. Am. J. Bot. *43*, 687–696.

Rick, C.M. (1956b). A new jointless gene from the Galapagos L. pimpinellifolium. TGC Report *6*, 23.

Robinson, R.W. (1980). Pleiotropic effects of the j-2 gene. TGC Report *30*, 32.

Robinson, M.D., McCarthy, D.J., and Smyth, G.K. (2010). edgeR: a Bioconductor package for differential expression analysis of digital gene expression data. Bioinformatics *26*, 139–140.

RTeam D.C. (2015). R Core Team (2015). R: A language and environment for statistical computing. R Found. Stat. Comput. Vienna, Austria. http://www.R-project.org/.

Shalit, A., Rozman, A., Goldshmidt, A., Alvarez, J.P., Bowman, J.L., Eshed, Y., and Lifschitz, E. (2009). The flowering hormone florigen functions as a general systemic regulator of growth and termination. Proc. Natl. Acad. Sci. USA *106*, 8392–8397.

Shang, L., Liang, Q., Wang, Y., Zhao, Y., Wang, K., and Hua, J. (2016). Epistasis together with partial dominance, over-dominance and QTL by environment interactions contribute to yield heterosis in upland cotton. Theor. Appl. Genet. *129*, 1429–1446.

Singh, R., Low, E.-T.L., Ooi, L.C.-L., Ong-Abdullah, M., Ting, N.-C., Nagappan, J., Nookiah, R., Amiruddin, M.D., Rosli, R., Manaf, M.A.A., et al. (2013). The oil palm SHELL gene controls oil yield and encodes a homologue of SEEDSTICK. Nature *500*, 340–344.

Soyk, S., Müller, N.A., Park, S.J., Schmalenbach, I., Jiang, K., Hayama, R., Zhang, L., Van Eck, J., Jiménez-Gómez, J.M., and Lippman, Z.B. (2017). Variation in the flowering gene SELF PRUNING 5G promotes day-neutrality and early yield in tomato. Nat. Genet. *49*, 162–168.

Stephenson, A.G. (1981). Flower and fruit abortion: proximate causes and ultimate functions. Annu. Rev. Ecol. Syst. *12*, 253–279.

Stubbe, H. (1972). Mutanten der Kulturtomate Lycopersicon esculentum Miller VI. Kulturpflanze *16*, 185–230.

Swinnen, G., Goossens, A., and Pauwels, L. (2016). Lessons from Domestication: Targeting Cis-Regulatory Elements for Crop Improvement. Trends Plant Sci. *21*, 506–515.

Tamura, K., Stecher, G., Peterson, D., Filipski, A., and Kumar, S. (2013). MEGA6: Molecular evolutionary genetics analysis version 6.0. Mol. Biol. Evol. *30*, 2725–2729.

Theißen, G., Melzer, R., and Rümpler, F. (2016). MADS-domain transcription factors and the floral quartet model of flower development: linking plant development and evolution. Development *143*, 3259–3271.

Tieman, D., Zhu, G., Resende, M.F.R., Jr., Lin, T., Nguyen, C., Bies, D., Rambla, J.L., Beltran, K.S.O., Taylor, M., Zhang, B., et al. (2017). A chemical genetic roadmap to improved tomato flavor. Science *355*, 391–394.

Vrebalov, J., Ruezinsky, D., Padmanabhan, V., White, R., Medrano, D., Drake, R., Schuch, W., and Giovannoni, J. (2002). A MADS-box gene necessary for fruit ripening at the tomato ripening-inhibitor (rin) locus. Science *296*, 343–346.

Weber, E., Engler, C., Gruetzner, R., Werner, S., and Marillonnet, S. (2011). A modular cloning system for standardized assembly of multigene constructs. PLoS One *6*, e16765.

Werner, S., Engler, C., Weber, E., Gruetzner, R., and Marillonnet, S. (2012). Fast track assembly of multigene constructs using Golden Gate cloning and the MoClo system. Bioeng. Bugs *3*, 38–43.

Williams, T.N., Mwangi, T.W., Wambua, S., Peto, T.E.A., Weatherall, D.J., Gupta, S., Recker, M., Penman, B.S., Uyoga, S., Macharia, A., et al. (2005). Negative epistasis between the malaria-protective effects of α+-thalassemia and the sickle cell trait. Nat. Genet. *37*, 1253–1257.

Xu, C., Liberatore, K.L., MacAlister, C.A., Huang, Z., Chu, Y.-H., Jiang, K., Brooks, C., Ogawa-Ohnishi, M., Xiong, G., Pauly, M., et al. (2015). A cascade of arabinosyltransferases controls shoot meristem size in tomato. Nat. Genet. *47*, 784–792.

Yang, T.J., Lee, S., Chang, S.-B., Yu, Y., de Jong, H., and Wing, R.A. (2005). In-depth sequence analysis of the tomato chromosome 12 centromeric region: identification of a large CAA block and characterization of pericentromere retrotranposons. Chromosoma *114*, 103–117.

Zahara, M.B., and Scheuerman, R.W. (1988). Hand-harvesting jointless vs. jointed-stem tomatoes. Calif. Agric. *42*, 14.

Zhang, L., Yang, G., Liu, P., Hong, D., Li, S., and He, Q. (2011). Genetic and correlation analysis of silique-traits in Brassica napus L. by quantitative trait locus mapping. Theor. Appl. Genet. *122*, 21–31.

Zhao, Q., Weber, A.L., McMullen, M.D., Guill, K., and Doebley, J. (2011). MADS-box genes of maize: frequent targets of selection during domestication. Genet. Res. *93*, 65–75.

STAR★METHODS

KEY RESOURCES TABLE

REAGENT or RESOURCE	SOURCE	IDENTIFIER
Biological Samples		
DNA and leaf tissue from tomato elite breeding lines.	See Table S2	N/A
Chemicals, Peptides, and Recombinant Proteins		
CTAB	Sigma Aldrich	Cat#H6269-500G
Agarose	VWR	Cat#97062-250
BsaI	NEB	Cat#R0535L
BpiI	Thermo Fisher	Cat#ER1012
T4 DNA Ligase	NEB	Cat#M0202L
Difco Yeast Nitrogen Base w/o Amino Acids	BD	Cat#291940
Do Supplement -Trp	Clonetech	Cat#630413
Do Supplement -Leu	Clonetech	Cat#630414
Do Supplement -Leu/-Trp	Clonetech	Cat#630417
Do Supplement -His/-Leu	Clonetech	Cat#630418
Do Supplement -Leu/-Trp/-His	Clonetech	Cat#630419
Do Supplement -Ade/-His/-Leu/-Trp	Clonetech	Cat#630428
3-Amino-1,2,4-triazole	Sigma Aldrich	Cat#A8056
Acetone	Fisher Scientific	Cat#A928-4
Taq DNA Polymerase with Standard Taq Buffer	NEB	Cat#M0273L
KOD Xtreme Hot Start DNA Polymerase	Millipore	Cat#71975
Critical Commercial Assays		
TruSeq DNA PCR-Free HT Library Preparation Kit	Illumina	Cat#FC-121-3003
TruSeq Nano DNA LT Library Preparation Kit	Illumina	Cat#FC-121-4001
Kapa Library quantification kit	Kapa Biosystems	Cat#07960140001
Matchmaker Gold Yeast Two-Hybrid System	Clontech	Cat#630489
RNase Free DNase Set	QIAGEN	Cat#79254
QIAprep Spin Miniprep Kit	QIAGEN	Cat#27106
QIAquick PCR Purification Kit	QIAGEN	Cat#28106
StrataClone Blunt PCR Cloning Kit	Stratagene	Cat#240207
SuperScript III First-Strand Synthesis System	Invitrogen	Cat#18080051
RNeasy Plant Mini Kit	QIAGEN	Cat#74904
ARCTURUS PicoPure RNA Isolation Kit	Thermo Fisher	Cat#KIT0204
Dynabeads mRNA Purification Kit	Thermo Fisher	Cat#61006
NEBNext Ultra RNA library prep kit for Illumina	NEB	Cat#E7530S
Deposited Data		
RNA-sequencing and whole-genome sequencing data	This study	SRP100435
RNA-seq data for WT M82	(Lemmon et. al., 2016)	SRP090200
RNA-seq data for s mutant	(Park et. al., 2012)	ftp://ftp.solgenomics.net
Experimental Models: Organisms/Strains		
Tomato wild species, landraces, and cultivars	See Table S1	N/A
Tomato elite breeding lines	See Table S2	N/A
Oligonucleotides		
Primer sequences for Y2H cloning, see **Table S4**	This study	N/A
Primer sequences for genotyping, see **Table S4**	This study	N/A

(*Continued on next page*)

Continued

REAGENT or RESOURCE	SOURCE	IDENTIFIER
Primer sequences for RT-PCR, see **Table S4**	This study	N/A
sgRNA sequences, see **Table S4**	This study	N/A
Primer sequences for sequencing, see **Table S4**	This study	N/A
Recombinant DNA		
MoClo Toolkit	(Weber et al., 2011)	Addgene #1000000044
pICH86966::AtU6p::sgRNA_PDS	(Belhaj et al., 2013)	Addgene #46966
pICH47732::NOSp::NPTII	(Belhaj et al., 2013)	Addgene #51144
pICH47742::35S::Cas9	(Belhaj et al., 2013)	Addgene #49771
Software and Algorithms		
Trimmomatic	(Bolger et al., 2014b)	http://www.usadellab.org/cms/?page=trimmomatic
Tophat2	(Kim et al., 2013)	https://ccb.jhu.edu/software/tophat/
Samtools	(Li et al., 2009)	http://www.htslib.org/
HTSeq-count	(Anders et al., 2015)	http://www-huber.embl.de/users/anders/HTSeq/doc/overview.html
R	(RTeam, 2015)	https://www.r-project.org/
EdgeR	(Robinson et al., 2010)	https://bioconductor.org/packages/release/bioc/html/edgeR.html
BWA-MEM	(Li, 2013; Li and Durbin, 2009)	http://bio-bwa.sourceforge.net/
PicardTools	N/A	http://broadinstitute.github.io/picard
Bcftools	(Li, 2011)	http://www.htslib.org/
MEGA6	(Tamura et al., 2013)	www.megasoftware.net/
MacVector 10.6.0	MacVector (2009)	http://macvector.com
Mfuzz	(Futschik, 2015)	http://www.sysbiolab.eu/software/R/Mfuzz/index.html

CONTACT FOR REAGENT AND RESOURCE SHARING

Further information and requests for resources and reagents should be directed to and will be fulfilled by the Lead Contact, Zachary B. Lippman (lippman@cshl.edu).

Material Transfer Agreements (MTA) were entered between Zachary B. Lippman and Monsanto, Syngenta, Bayer Crop Science, and Lipman Seeds that restrict the distribution of all DNA, tissue, or seed for elite tomato cultivars listed in Table S2.

EXPERIMENTAL MODEL AND SUBJECT DETAILS

Plant material and growth conditions

Seeds of the standard *S. lycopersicum* cultivar M82 (LA3475) were from our own stocks. Core collection germplasm (https://www.eu-sol.wur.nl) was from the seed stocks of Z. Lippman, D. Zamir, and S. Huang (Lin et al., 2014). Seeds of the jointless accessions were obtained from the Charles M. Rick Tomato Genetics Resource Center (TGRC) at the University of California, Davis (Table S1). The *frondea* mutant was obtained from the gene bank of the Leibniz Institute of Plant Genetics and Crop Plant Research (IPK) in Gatersleben, Germany. Seed of the *long inflorescence* (*lin*) mutant in the Micro-tom background (TOM-JPG5091) was provided by the University of Tsukuba, Gene Research Center, through the National Bio-Resource Project (NBRP) of the AMED, Japan (http://tomatoma.nbrp.jp/). We backcrossed the *lin* mutant four times to our standard M82 cultivar. The landrace collection (*S. lycopersicum* var. *cerasiforme*) was from the seed stocks of E. van der Knaap. We obtained tissue samples, DNA, or seed of elite breeding lines from Syngenta, Nunhems, Monsanto, Lipman Seeds, Johnny's Seeds, and TomatoGrowers. All accessions used in this study are listed in Tables S1 and S2.

Seeds were either pre-germinated on moistened Whatman paper at 28°C in complete darkness or directly sown and germinated in soil in 96-cell plastic flats. Plants were grown under long-day conditions (16-h light/8-h dark) in a greenhouse under natural light supplemented with artificial light from high-pressure sodium bulbs (~250 μmol m^{-2} s^{-1}). Daytime and nighttime temperatures were 26–28 °C and 18–20 °C, respectively, with a relative humidity of 40%–60%.

Analyses of inflorescence architecture, sepal length, fruit type, and productivity traits were conducted on plants grown in the fields at Cold Spring Harbor Laboratory, Cold Spring Harbor, New York, the Cornell Long Island Horticultural Experiment Station in Riverhead, New York, and net houses in Hatzav, Israel. Analyses of sepal length in the landraces were conducted on plants grown in the fields of the Durham horticulture farm at the University of Georgia, Athens, Georgia. Seeds were germinated in 96-cell flats and grown for 32 d in the greenhouse before being transplanted to the field. Plants were grown under drip irrigation and standard fertilizer regimes. Damaged or diseased plants were marked throughout the season and were excluded from the analyses.

METHOD DETAILS

Plant phenotyping

For analyses of sepal length, we manually measured the length of sepals and petals of 10 closed flower buds per accession and calculated the sepal/petal ratio. Mature floral buds of similar developmental stage were collected (1-2 days before anthesis, i.e., before flower opening). For analyses of inflorescence complexity, we counted the number of branching events on at least 5 inflorescences on each replicate plant.

Yeast two-hybrid analysis

Protein interaction assays in yeast were performed using the Matchmaker Gold Yeast Two-Hybrid System (Clontech) as described before (Park et al., 2014b). The coding sequences for bait proteins were cloned into the pGBKT7 vector, and the resulting vectors were transformed into the Y2HGold yeast strain. The coding sequences for prey proteins were cloned into the pGADT7 AD vector, and the resulting vectors were transformed into the Y187 yeast strain. After mating the two yeast strains expressing bait and prey proteins, diploid yeast cells were selected and grown on dropout medium without leucine and tryptophan. To assay protein-protein interactions, clones were grown on triple-dropout medium without leucine, tryptophan, and histidine for 3 d at 30°C. To block autoactivation, we added 3 mM 3-amino-1,2,4-triazole (3-AT) or removed adenine from the triple-dropout medium. All primer sequences used for cloning can be found in Table S4.

Meristem imaging

Live meristems were imaged using a Nikon SMZ1500 stereomicroscope (Nikon). Shoot apices were dissected from seedlings and older leaf primordia were removed to expose meristems. Immediately after dissection, sequences of optical layers were imaged using a Nikon DS-Ri1 digital camera (Nikon) mounted on the stereomicroscope. Z stacks of optical sections were aligned and merged to produce final focused images using the NIS Elements BR3.2 software (Nikon).

Meristem transcriptome profiling

Meristem collection, RNA extraction, and library preparation for *s2* mutant plants was performed as previously described (Park et al., 2012). Briefly, we collected seedling shoots at the vegetative meristem (VM), transition meristem (TM), sympodial inflorescence meristem (SIM), and floral meristem (FM) stage of meristem maturation, and immediately fixed them in ice-cold acetone. Meristems were manually dissected under a stereoscope and two biological replicates consisting of 30-50 meristems from independent plants were generated. Total RNA was extracted with the PicoPure RNA Extraction kit (Arcturus) and mRNA was purified with Dynabeads mRNA Purification kits (Thermo Fisher). Barcoded libraries were prepared using the NEBNext Ultra RNA library prep kit for Illumina according to the manufacturer's instructions, and assessed for size distribution and concentration with a Bioanalyzer 2100 (Agilent) and the Kapa Library quantification kit (Kapa Biosystems), respectively. Libraries were sequenced on a single Illumina Hiseq 2500 lane (222,279,510 million paired-end reads) at the Genome Center of Cold Spring Harbor Laboratories, Cold Spring Harbor.

Previously collected reads for wild-type tomato cultivar M82, *compound inflorescence* (*s*) mutant (Lemmon et al., 2016; Park et al., 2012), and reads for the *s2* mutant were trimmed by quality using Trimmomatic (Bolger et al., 2014b) and aligned to the reference genome sequence of tomato (SL2.50) (Consortium, 2012) using Tophat2 (Kim et al., 2013). Alignments were sorted with samtools (Li et al., 2009) and gene expression quantified as unique read pairs aligned to reference annotated gene features (ITAG2.4) using HTSeq-count (Anders et al., 2015).

All statistical analyses of gene expression were conducted in R (RTeam, 2015). Expression of individual genes is shown as transcripts per million (TPM). Significant differential expression between meristem stages in wild-type tomato cultivar M82 was identified for 2,582 genes with edgeR (Robinson et al., 2010) using 2-fold change, average 1 CPM, and FDR $\leq$ 0.10 cutoffs (Lemmon et al., 2016). To compare expression dynamics by principal component analysis (PCA), we used *z*-score normalization of raw counts within genotype to minimize the impact of the different sequencing lengths (50 bp versus 100 bp) and platforms (GAIIx and HiSeq2500). PCA was conducted on normalized expression values for the 2,582 dynamic genes in wild-type tomato cultivar M82, *s*, and *s2* using the prcomp function in R (RTeam, 2015). The first two principal components were then plotted to assess acceleration or delay of the meristem maturation process in mutant samples. The proportion of TM and FM marker genes with moderate and severely delayed expression was assessed by a two-step *k*-means clustering. First, normalized WT expression was grouped into twelve clusters and the two clusters with the most specific TM and FM expression were designated as markers. Mutant expression from TM and

FM marker genes was normalized with WT, producing WT:*s* and WT:*s2* normalized expression datasets. Finally, *k*-means clustering (12 clusters) was performed on *s* and *s2* normalized expression alone and clusters with delays in activation compared to WT were identified by hand.

Mapping-by-sequencing

To map the causal mutations in the *s2* mutant, we generated two second-generation (F_2) populations by crossing *s2* with the *S. lycopersicum* cultivar M82, and *s2* with *S. pimpinellifolium*. From a total of 464 *s2* × M82 F_2 plants, we selected 25 *s2* mutants, 20 *j2* mutants, and 13 WT siblings for tissue collection, nuclei isolation, and DNA extraction. An equal amount of tissue from each plant (~0.2 g) was pooled for DNA extraction using standard protocols. Libraries were prepared with the Illumina TruSeq DNA PCR-free prep kit from 2 μg genomic DNA sheared to 550 bp insert size. From a total of 576 *s2* × *S. pimpinellifolium* F_2 plants, we selected 16 *s2* mutants, 9 *j2* mutants, and 13 wild-type siblings for DNA extraction. We also extracted DNA from the *s2* parent (LA4371). Libraries were prepared with the Illumina TruSeq Nano DNA prep kit from 200 ng genomic DNA sheared to 550 bp insert size and 8 cycles of final amplification. We sequenced all DNA libraries on an Illumina NextSeq platform at the Cold Spring Harbor Laboratory Genome Center (Woodbury, NY). For the *s2* × M82 F_2 population, we obtained 62,317,992, 73,496,741, and 79,699,274 paired-end 151-bp reads for the *s2* mutant, *j2* mutant, and the WT sibling samples, respectively. For the *s2* × *S. pimpinellifolium* F_2 population, we obtained 32,979,728, 82,439,796, and 50,763,441 paired-end 151-bp reads for pools of *s2*, *j2*, and the WT siblings, respectively. For the *s2* parent we obtained 48,281,689 paired-end 151-bp reads.

To map the causal mutation in the *lin* mutant, we generated a F_2 population by crossing the *lin* mutant with *S. pimpinellifolium*. From a total of 216 F_2 plants, we selected 8 *lin* mutant plants with the most strongly branched inflorescences and 17 WT siblings for tissue collection. An equal amount of tissue from each plant (~0.2 g) was pooled for nuclei isolation and DNA extraction using standard protocols. Barcoded libraries were prepared with the Illumina TruSeq DNA PCR-free prep kit from 2 μg genomic DNA sheared to 550 bp insert size and sequenced as above. We obtained 4,624,816 and 5,063,861 paired-end 101-bp reads for the *lin* mutant and the WT sibling pools, respectively. To find the *lin* mutation, we resequenced a pool of 7 *lin* × *S. pimpinellifolium* F_2 mutant plants on the Illumina HiSeq2500 platform, and obtained an additional 161,827,433 paired-end 101-bp reads.

To map *s2* suppressor loci in *S. pimpinellifolium*, we regrew 1,536 *S. pimpinellifolium* × *s2* F_2 plants and selected 92 homozygous $j2^{TE}$ $ej2^{w}$ double mutants by PCR genotyping. Primers are listed in Table S4. We selected 18 *s2* mutants, 6 moderately suppressed *s2* mutants, and 2 strongly suppressed *s2* mutants for tissue collection, nuclei isolation, and DNA extraction. Libraries were prepared with the Illumina TruSeq DNA PCR-free prep kit from 2 μg genomic DNA sheared to 550 bp insert size, and sequenced as above. We obtained 38,060,212, 38,044,727 and 52,426,078 paired-end 151-bp reads for the pools of *s2*, moderately suppressed *s2*, and the strongly suppressed *s2* plants, respectively.

Genomic DNA reads were trimmed by quality using Trimmomatic (Bolger et al., 2014b) and paired reads mapped to the reference tomato genome (SL2.50) using BWA-MEM (Li, 2013; Li and Durbin, 2009). Alignments were then sorted with samtools and duplicates marked with PicardTools (Li et al., 2009, http://broadinstitute.github.io/picard). SNPs were called with samtools/bcftools (Li, 2011; Li et al., 2009) using read alignments for the various genomic DNA sequencing pools from this project in addition to reference M82 (Bolger et al., 2014a) and *S. pimpinellifolium* (Consortium, 2012) reads. Called SNPs were then filtered for bi-allelic high quality SNPs at least 100 bp from a called indel using bcftools (Li, 2011). Following read alignment and SNP calling, all statistics and calculations were done in R (RTeam, 2015). Read depth for each allele at segregating bi-allelic SNPs in 1 Mb sliding windows (by 100 kb) was summed for the various mutant (*s2*, $j2^{TE}$, or suppression of *s2*) and wild-type sequencing pools and mutant:non mutant SNP ratios were calculated. Finally, mutant SNP ratio was divided by wild-type SNP ratio (+ 0.5) and plotted across the 12 tomato chromosomes.

Tissue collection and RNA extraction

For semiquantitative RT-PCR, seeds were germinated on moistened Whatman paper at 28°C in complete darkness. Seedlings at similar germination stages were transferred to soil in 72-cell plastic flats and grown in the greenhouse. Shoot apices were collected at the floral meristem (FM) stage of meristem maturation (Park et al., 2012), and immediately flash-frozen in liquid nitrogen. Total RNA was extracted using the RNeasy Plant Mini Kit (QIAGEN) and treated with the RNase Free DNase Set (QIAGEN), or the Arcturus PicoPure RNA Extraction kit (Thermo Fisher) according to the manufacturer's instructions. 100 ng to 1 μg of total RNA was used for cDNA synthesis using the SuperScript III First-Strand Synthesis System (Invitrogen). All primer sequences can be found in Table S4.

Phylogenetic analyses and sequence analyses

Sequences of tomato and *Arabidopsis* SEP family members were obtained from the Phytozome v11 database (https://www.phytozome.jgi.doe.gov) and aligned using the ClustalW function in MEGA. Phylogenetic trees for proteins with 1,000 bootstrap replicates were constructed using the maximum likelihood method in MEGA6 (Tamura et al., 2013). Homologous proteins in the clades containing *Arabidopsis* SEP1/2, SEP3, and SEP4 were assigned as SEP1/2-, SEP3-, and SEP4-homologs, respectively.

For analyzing linkage between *EJ2* and *FW3.2*, we genotyped the M9 SNP at position SL2.50ch03:64799226 (Chakrabarti et al., 2013) (G in *S. pimpinellifolium* (*FW3.2*) and A in *S. lycopersicum* cv. M82 (*fw3.2*)) in accessions of our tomato core collection using published genome sequencing data (Lin et al., 2014; Tieman et al., 2017).

CRISPR/Cas9 mutagenesis, plant transformation, and selection of mutant alleles

CRISPR/Cas9 mutagenesis and generation of transgenic plants was performed following our standard protocol (Belhaj et al., 2013; Brooks et al., 2014). Briefly, two single-guide (sg)RNAs binding in the coding sequence of the target gene were designed using the CRISPR-P tool (http://cbi.hzau.edu.cn/cgi-bin/CRISPR) (Lei et al., 2014). Vectors were assembled using the Golden Gate cloning system (Werner et al., 2012). The sgRNA-1 and sgRNA-2 were cloned downstream of the *Arabidopsis* U6 promoter in the Level 1 acceptors pICH47751 and pICH47761, respectively. The Level1 constructs pICH47731-NOSpro::NPTII, pICH47742-35S:Cas9, pICH47751-AtU6pro:sgRNA-1, and pICH47761-AtU6::sgRNA-2 were assembled in the binary Level 2 vector pAGM4723. Fifteen-μl restriction-ligation reactions were performed in a thermocycler (3 min at 37°C and 4 min at 16° for 20 cycles, 5 min at 50°C, 5 min at 80°C, and final storage at 4°C). All sgRNA sequences are listed in Table S4.

Final binary vectors were transformed into the tomato cultivar M82 and the tomato wild species *S. pimpinellifolium* by *Agrobacterium tumefaciens*-mediated transformation (Gupta and Van Eck, 2016). After *in-vitro* regeneration, culture medium was washed from the root system and plants transplanted into soil. For acclimation, plants were covered with transparent plastic domes and maintained in a shaded area for 5 days. A total of 8 first-generation (T_0) transgenics were genotyped for induced lesions using forward and reverse primer flanking the sgRNA target sites. PCR products were separated on agarose gels and selected products were cloned into pSC-A-amp/kan vector (StrataClone Blunt PCR Cloning Kit, Stratagene). At least 6 clones per PCR product were sequenced using M13-F and M13-R primer. T_0 plants with lesions were backcrossed to wild-type and the F_1 generation was genotyped for desirable large deletion alleles and presence/absence of the CRISPR/Cas9 transgene using primer binding the 3′ of the 35S promoter and the 5′ of the Cas9 transgene, respectively. All primers are listed in Table S4. Plants heterozygous for the engineered deletion alleles and lacking the transgene were self-pollinated to isolate homozygous, non-transgenic null mutants from the F_2 generation.

Generation of parental and hybrid lines for cherry tomato breeding and yield trials under agricultural greenhouse conditions

To test the potential of *j2 ej2* and *s* genotypes for fresh-market tomato breeding, hybrids were generated by crossing near-isogenic lines isolated from a breeding population that was developed for breeding high-yielding, indeterminate cherry tomato cultivars with a range of fruit shapes (Dani Zamir). Depending on genotype, near-isogenic lines were generated by backcrossing once to the respective cherry parents (BC_1) followed by inbreeding for 3 generations (F_3) or by inbreeding for 3-6 generations (F_3-F_6). Fruit shapes, inflorescence types, and yield characteristics were evaluated and selected each generation. Ten replicate plants per parental and hybrid line were grown in a randomized plot design in net houses in Hatzav, Israel in the year 2017. Damaged or diseased plants were marked throughout the season and were excluded from the analyses.

j2 ej2 hybrid experiment

A jointless ($j2^{TE}$) processing inbred (F_6) wild-type for *EJ2* (*j2 EJ2*) served as parent (P-6022) for generating test and control hybrids. Test parents were isolated from a jointless ($j2^{TE}$) cherry inbred population (BC_1F_3), which segregated for $ej2^{w}$. Two $j2^{TE}$ parents (P-6086-2 and P-6086-9) and two $j2^{TE}$ $ej2^{w}$ parents (P-6086-4 and P-6086-8) were selected by $ej2^{w}$ genotyping, and were crossed to P-6022. Control hybrids were generated by crossing the $j2^{TE}$ test parents (P-6086-2 for trail-1 and P-6086-9 for trial-2) to the $j2^{TE}$ parent (P-6022). Test hybrids were generated by bulk crossing the $j2^{TE}$ $ej2^{w}$ test parents (P-6086-4 for trail-1 and P-6086-8 for trial-2) to the $j2^{TE}$ parent (P-6022).

s hybrid experiment

An indeterminate cocktail inbred (F_3) and a determinate cherry inbred (F_3) served as parents (P-6097 and P-6105, respectively) for generating test and control hybrids. Test parents were isolated from an indeterminate cherry-type F_5 inbred line that segregated the *s* mutation. One parent wild-type for *S* (P-6089) and one *s* mutant parent (P-6090) were selected by phenotyping and self-fertilized. The F_6 generation was stable for unbranched (P-6089) and compound inflorescences (P-6090). Control and test hybrids were generated by bulk crossing the *S* parents (P-6097 for trail-1 and P-6105 for trial-2) to the *S* (P-6089) and the *s* (P-6090) test parents, respectively.

For analyses of yield component traits, mature green (MG) and red fruits (MR) were collected from 6 subsequent individual inflorescences and MG fruit number (MGFN), MR fruit number (MRFN), MG fruit weight (MGFW), and MR fruit weight (MRFW) was determined per inflorescence. Total fruit number (TFN) was the sum of MGFN and MRFN from each plant. Total yield (TY) was the sum of MGFW and MRFW from each plant. The average fruit weight (FW) was calculated by dividing MRFW by MRFN. From each plant, 7-10 fruits from at least one inflorescence were randomly selected to determine total soluble sugar content (Brix) in fruit juice. Brix value (percent) was quantified with a digital Brix refractometer (ATAGO Palette). For each measured yield parameter, mean values and percentage difference to the control hybrid were statistically compared using two tailed, two-sample t tests.

QUANTIFICATION AND STATISTICAL ANALYSES

Sampling

For quantitative analyses of flower number per inflorescence and inflorescence internode length, at least 10 inflorescences were analyzed per genotype. For quantitative analyses of inflorescence complexity at least 5 inflorescences each from 6 individual replicate plants were analyzed per genotype. For quantitative analyses of relative sepal length, at least 10 flowers were analyzed per genotype or ecotype. Hybrid inflorescence traits (number of branching events per inflorescence, total number of branches and flowers per plant) were determined for 6 subsequent inflorescences per individual plant and 9-10 individual plants per hybrid line. Total number of

mature green and red fruits per individual plant was determined from 6 subsequent inflorescences per plant and 9-10 individual plants per hybrid line. Exact numbers of individuals (*N*) are presented in all figures. Statistical calculations were performed using R and Microsoft Excel. Mean values for each measured parameter were compared using two-tailed, two-samples Student's t test.

Transcriptome quantification

Reads for the wild-type M82, *compound inflorescence* (*s*) mutant (Lemmon et al., 2016; Park et al., 2012), and the *s2* mutant were trimmed by quality using Trimmomatic v0.32 (HiSeq2500 parameters: ILLUMINACLIP:TruSeq3-PE-2.fa:2:40:15:1:FALSE LEADING:3 TRAILING:3 SLIDINGWINDOW:4:15 MINLEN:36; GAIIx parameters: ILLUMINACLIP:TruSeq2-PE.fa:2:30:10:1:FALSE LEADING:3 TRAILING:3 SLIDINGWINDOW:4:15 MINLEN:36 TOPHRED33) (Bolger et al., 2014b) and aligned to the reference genome sequence of tomato (SL2.50) (Consortium, 2012) using Tophat2 v2.0.127 (parameters:–b2-very-sensitive–read-mismatches 2–read-edit-dist 2–min-anchor 8–splice-mismatches 0–min-intron-length 50–max-intron-length 50000–max-multihits 20) (Kim et al., 2013). Alignments were sorted with samtools (Li et al., 2009) and gene expression quantified as unique read pairs aligned to reference annotated gene features (ITAG2.4) using HTSeq-count v0.6.08 (parameters:–format = bam–order = name–stranded = no–type = exon–idattr = Parent) (Anders et al., 2015).

All statistical analyses of gene expression were conducted in R (RTeam, 2015). Significant differential expression between meristem stages in wild-type M82 was identified for 2,582 genes with edgeR (Robinson et al., 2010) using 2-fold change, average 1 CPM, and FDR $\leq$ 0.10 cutoffs (Lemmon et al., 2016). To compare expression dynamics between genotypes, we used *z*-score normalization within genotype to minimize the impact of the different sequencing lengths (50 bp versus 100 bp) and platforms (GAIIx and HiSeq2500). A principal component analysis (PCA) was conducted on these normalized expression values for the 2,582 dynamic genes including wild-type M82, *s*, and *s2* using the prcomp function in R (RTeam, 2015). The first two principal components were then plotted to assess modified maturation schedules in the mutant samples. The proportion of TM and FM marker genes with moderate and strongly delayed expression was assessed by a two-step *k*-means clustering. First, WT expression (TPM) was *z*-score normalized and clustered into twelve groups using the kmeans2 function from the Mfuzz package (Futschik, 2015) in R. The two clusters with the most specific TM and FM expression (clusters 06 and 08, respectively; Figure S2A) were designated as marker clusters. Mutant *s* and *s2* expression (TPM) from the 277 TM and 241 FM marker genes was *z*-score normalized with WT expression, producing a WT:*s* normalized expression and WT:*s2* normalized expression dataset. Finally, *k*-means clustering (12 clusters) was performed on *s* (Figure S2B) and *s2* (Figure S2C) expression alone (normalized by WT expression levels) and clusters with moderate and severe delays in activation compared to WT were manually identified.

Mapping

For mapping-by-sequencing of the various mutants, reads were trimmed by quality using Trimmomatic v0.32 (HiSeq 2500 read parameters: ILLUMINACLIP:TruSeq3-PE-2.fa:2:40:15:1:FALSE LEADING:3 TRAILING:3 SLIDINGWINDOW:4:15 MINLEN:36 ; GAIIx read parameters: ILLUMINACLIP:TruSeq2-PE.fa:2:30:10:1:FALSE LEADING:3 TRAILING:3 SLIDINGWINDOW:4:15 MINLEN:36 TOPHRED33) and paired reads mapped to the reference tomato genome (SL2.50) using BWA-MEM v0.7.10-r789 (parameters: -M) (Li, 2013). Alignments were then sorted with samtools and duplicates marked with PicardTools v1.126 (parameters: VALIDATION_STRINGENCY = LENIENT) (Li et al., 2009, http://broadinstitute.github.io/picard). SNPs were called with samtools/bcftools v1.3.1 (samtools mpileup parameters:–ignore-RG–max-depth 1000000–output-tags DP,AN–min-BQ 0–no-BAQ–uncompressed–BCF; bcftools call parameters:–multiallelic-caller–variants-only–output-type z) (Li, 2011; Li et al., 2009) using read alignments for the various sequencing pools from this project in addition to reference M82 (Bolger et al., 2014a) and *S. pimpinellifolium* (Consortium, 2012) reads. Called SNPs were then filtered for bi-allelic high quality (MQ > = 50) SNPs at least 100 bp from a called indel using bcftools (Li, 2011). Following read alignment and SNP calling and filtering, all mapping statistics and calculations were done using R (RTeam, 2015). Read depth for each allele at segregating bi-allelic SNPs in 1 Mb sliding windows (by 100 kb) was summed for the various mutant (*lin*, *s2*, *j2*, suppression of *s2*) and wild-type sequencing pools and mutant:non mutant SNP ratios were calculated. Finally, mutant SNP ratio was divided by wild-type SNP ratio (+ 0.5) and plotted across the tomato genome.

DATA AND SOFTWARE AVAILABILITY

The accession number for the RNA-sequencing and whole-genome sequencing data reported in this paper is Sequence Read Archive: SRP100435.

ADDITIONAL RESOURCES

Tomato core collection: https://unity.phenome-networks.com
CRISPR design: http://cbi.hzau.edu.cn/cgi-bin/CRISPR
Sequence retrieval: https://phytozome.jgi.doe.gov/
Data deposition: https://ncbi.nlm.nih.gov/sra

Cell

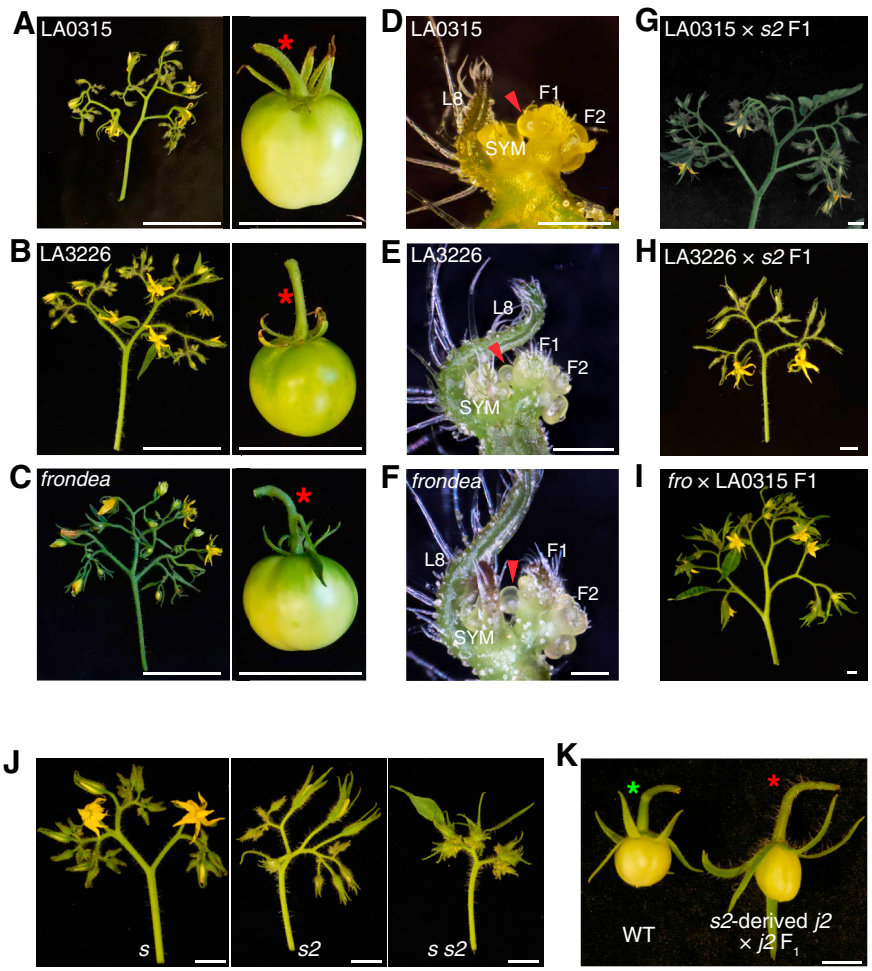

Figure S1. The *s2* Inflorescence Branching Variants Are Allelic, Fail to Complement the Classical *j2* Mutant, and Are Genetically Additive with *s*, Related to Figure 1

(A–C) The accessions LA0315 (A), LA3226 (B), and the X-ray-induced mutant *frondea* (C) (Stubbe, 1972) develop highly proliferated inflorescences that bear flowers and fruits with jointless pedicels (red asterisks).

(D–F) Stereoscope images of primary meristems in LA0315 (D), LA3226 (E), and *frondea* (F), showing the first inflorescence branching event (red arrowhead) at the base of the first flower (F1). SYM: sympodial shoot meristem; L8: leaf 8.

(G–I) Representative inflorescences of F_1 progeny from the crosses LA0315 × *s2* (G), LA3226 × *s2* (H), and *fro* × LA0315 (I) showing all four accessions (mutants) are allelic.

Scale bars in (A–C, G–I) and (D–F) indicate 5 cm and 500 μm, respectively.

(J) Inflorescences of *s* (left), *s2* (middle), and the *s s2* higher-order mutant (right). Greater inflorescence complexity in the *s s2* higher-order mutant suggests additivity.

(K) Complementation test using an *s2*-derived jointless mutant plants and the classical *j2* mutant. Jointed fruits (green asterisk) of WT plants and jointless fruits (red asterisk) of F_1 progeny from a cross of *s2*-derived *j2* and *j2* are shown. Scale bar = 1 cm.

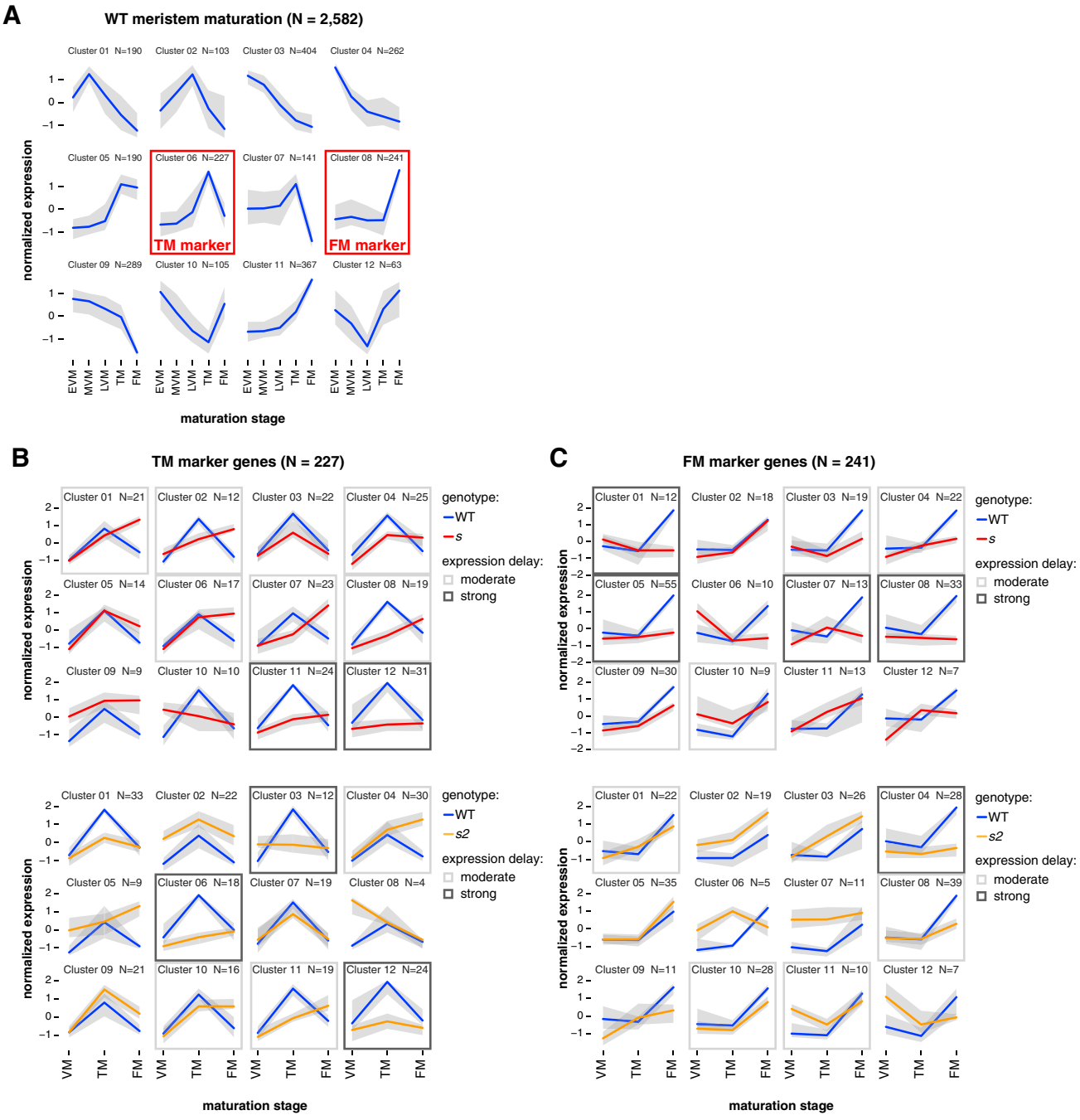

Figure S2. The Rate of Meristem Maturation in *s2* Mutants Is Less Delayed than in *s*, Related to Figure 1

(A) Clustering of 2,582 genes that were dynamically expressed during the early (EVM), middle (MVM), and late (LVM) vegetative meristem, the transition meristem (TM) and floral meristem (FM) stage of meristem maturation in the WT (see STAR Methods). Genes in Cluster 06 and Cluster 08 (red boxes) were selected as TM and FM marker genes, respectively. Colored lines indicate median expression with gray area representing the 5th and 95th quantile. N = number of genes.

(B) WT, *s* (top), and *s2* (bottom) *z*-score normalized expression of TM marker genes in vegetative (VM), transition (TM), and floral (FM) meristem stages. Cluster in light gray and dark gray boxes were selected as moderately and strongly delayed genes, respectively.

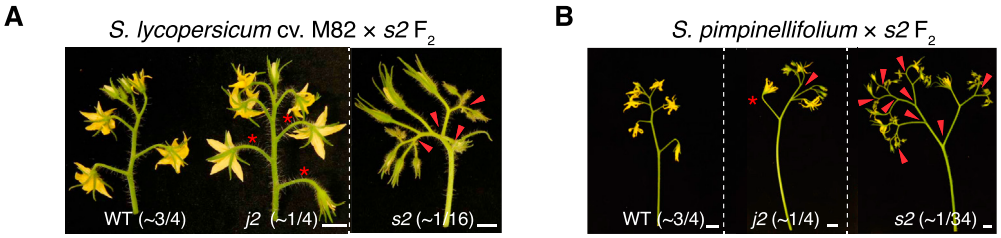

C

Population	total	*s2*	ratio
S.lyc × *s2* F_2	464	30	~1/16
S.pim × *s2* F_2	576	17	~1/34

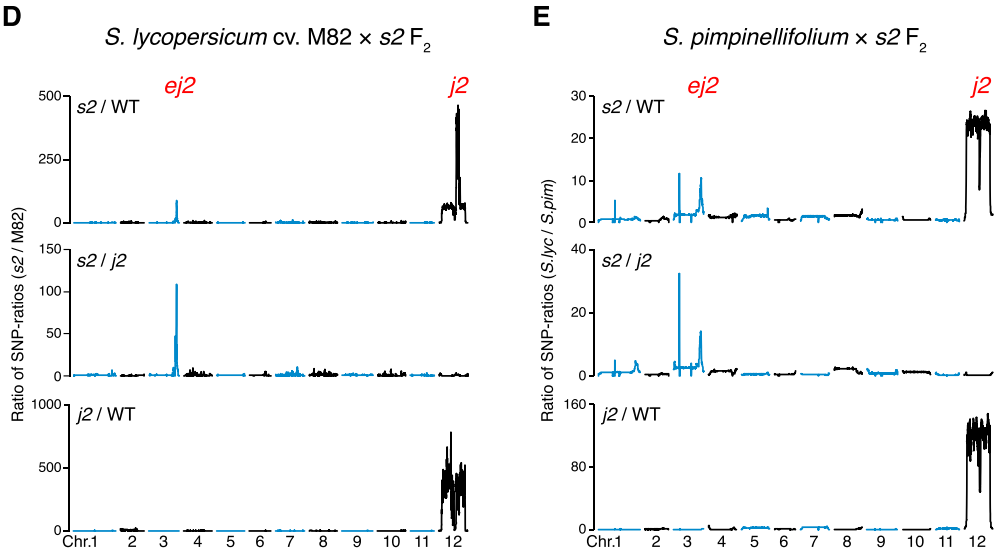

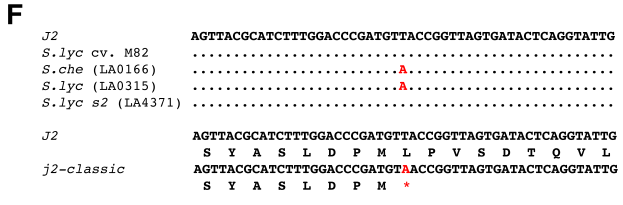

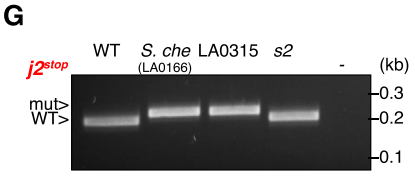

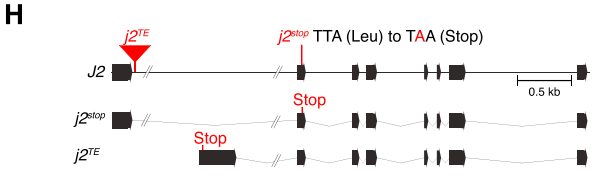

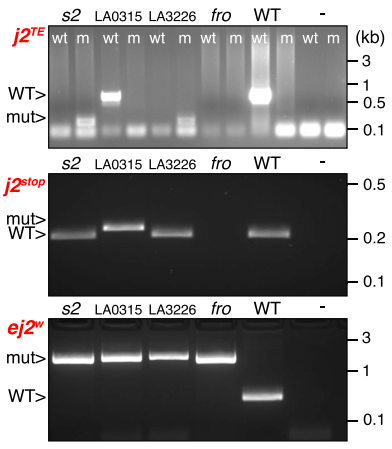

(legend on next page)

Figure S3. Mapping-by-Sequencing Reveals *s2* Branching Is Caused by Mutations in Two Tomato Homologs of the *SEPALLATA* MADS-Box Genes (*J2* and *EJ2*), Related to Figure 2

(A and B) Representative images of the phenotypic classes found in the M82 × *s2* F_2 (A) and *S. pimpinellifolium* × *s2* F_2 populations (B). Red asterisks mark jointless pedicels and red arrowheads mark inflorescence branching events. Scale bars = 1 cm.

(C) Segregation ratios of the *s2* branching phenotype in the two F_2 populations. Note that in the M82 × *s2* F_2, the *j2* and *s2* phenotypes segregated 1/4 and 1/16, respectively.

(D) Mapping-by-sequencing of the loci underlying *s2* in an M82 × *s2* F_2 population. Pooled DNA from WT, *j2* and *s2* plants was sequenced and the ratios of the SNP-ratios (*s2*/M82) between different phenotypic classes (top: *s2*/WT; middle: *s2*/*j2*; bottom: jointless/WT) are shown.

(E) Mapping-by-sequencing of the loci underlying *s2* in a *S. pimpinellifolium* × *s2* F_2 population. Pooled DNA from WT, *j2*, and *s2* plants was sequenced and ratios of the SNP-ratios (*S.lyc*/*S.pim*) are shown as in (D).

(F) Partial sequence alignment of *J2* (*Solyc12g038510*) from M82, the jointless *S. cheesmaniae* (*S. che*) accession LA0166, the classical *j2* accession (LA0315) and the *s2* accession (LA4371). A *S. cheesmaniae* SNP in the second exon leads to a premature stop-codon (asterisk). Allele designated as $j2^{stop}$.

(G) CAPS marker PCR genotyping assay for $j2^{stop}$ in accessions from (F). Positions of WT and mutant (mut) bands are indicated.

(H) Gene models showing the position of the *Copia*/*Rider* transposable element (TE) insertion in $j2^{TE}$ and the *S. cheesmaniae* SNP in $j2^{stop}$. Predicted RNA transcripts are shown below. The $j2^{stop}$ allele results in a premature stop codon in the second exon. The $j2^{TE}$ allele results in an intronic transcriptional start site and an early stop codon.

(I) Representative inflorescences of WT, $ej2^{w}$, $ej2^{CR}$, and $ej2^{CR}$ × $ej2^{w}$ F_1 progeny are shown. Scale bar = 1 cm.

(J) Genotyping of *s2*, LA0315, LA3226, *frondea* (*fro*), and WT plants using diagnostic PCR markers for $j2^{TE}$, $j2^{stop}$, and $ej2^{w}$. Note that both *s2* and LA3226 carry the $j2^{TE}$ and $ej2^{w}$ alleles, whereas LA0315 carries $j2^{stop}$ and $ej2^{w}$. The *frondea* mutant carries $ej2^{w}$, however, failed *J2* amplification in *frondea* using both *j2* markers suggest a large structural variant has disrupted the gene (SV). Band sizes are in kilobase pairs (kbp).

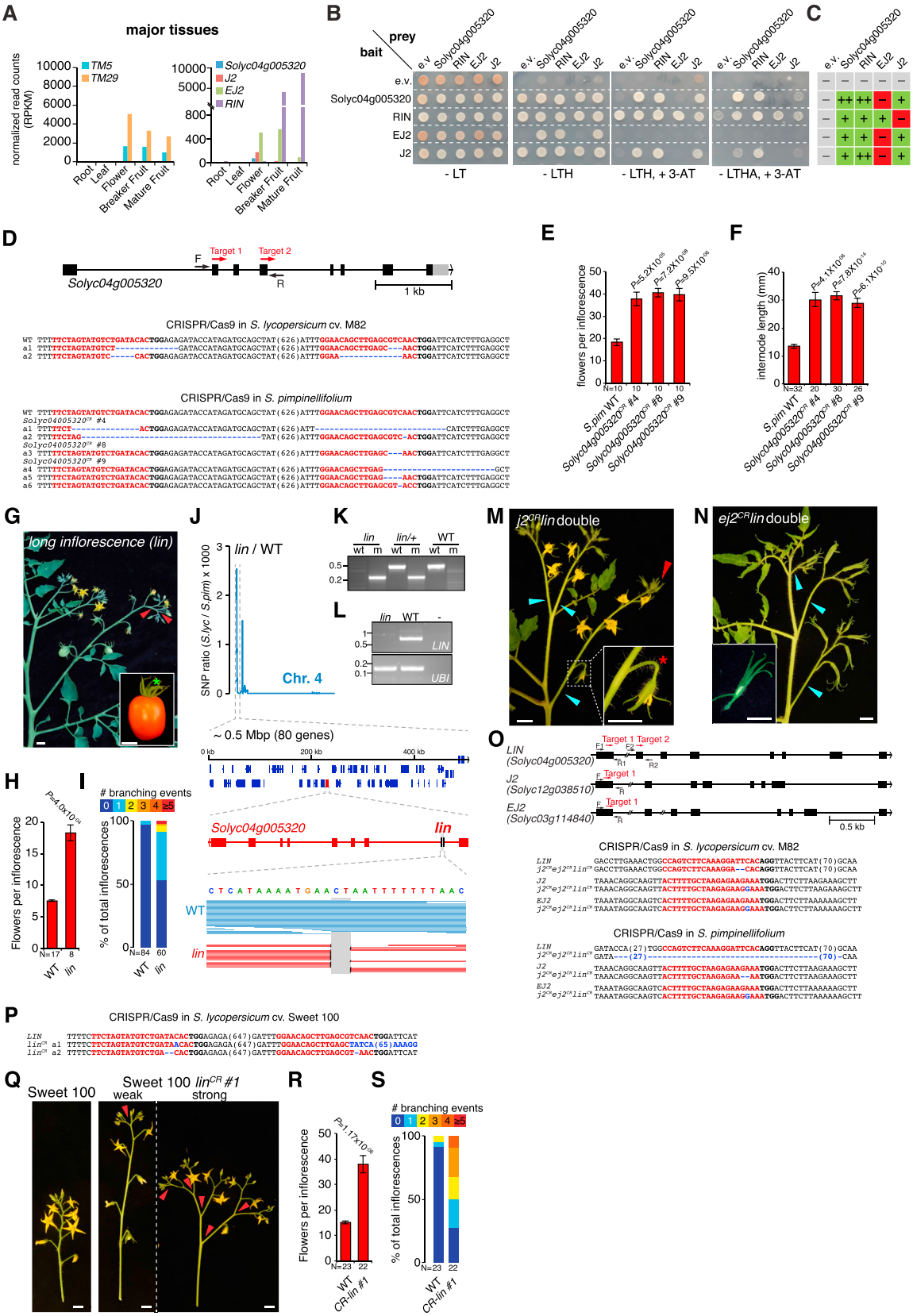

(legend on next page)

Figure S4. The Three *SEP4* Genes *J2*, *EJ2*, and *Solyc04g005320*/*LIN* Interact to Regulate Branching and Flower Development, Related to Figure 5

(A) Normalized gene expression (RPKM) for *TM5* and *TM29* (left) and the *SEP4* sub-clade (right) in major tissues.

(B) Yeast two-hybrid assays showing heteromeric interaction of Solyc04g005320, RIN, J2, and EJ2, and homomeric interaction of Solyc04g005320, RIN and J2 (3-AT, 3-amino-1,2,4-triazole; L, leucine; T, tryptophan; H, histidine; A, adenine; e.v., empty vector).

(C) Summary of results in (B); (-) no interaction; (+) interaction; (++) strong interaction.

(D) CRISPR/Cas9 targeting of *Solyc04g005320*. Sequences of *Solyc04g005320*^{CR} allele 1 (a1) and a2 in *S. lycopersicum* cv. M82 are shown (top). Three independent first-generation (T_0) chimeric *S. pimpinellifolium* transgenics were sequenced and 5 reads were obtained per plant (bottom). All sequenced alleles carried mutations, revealing putative biallelic (T_0 #4), homozygous (T_0 #8), and chimeric (T_0 #9) plants.

(E) Quantification of flowers per inflorescence for WT and 3 independent *lin*^{CR} T_0 transgenics. N = number of inflorescences.

(F) Quantification of internode length between flowers of the same plants as in (E). N = number of internodes.

(G) Representative *lin* mutant plant with elongated and weakly branched inflorescences. Red arrowheads indicate branch points. Inset shows *lin* fruit with jointed pedicel.

(H) Quantification of flowers per inflorescence for WT and *lin*. N = number of inflorescences.

(I) Quantification of inflorescence branching events in WT and *lin*.

(J and K) Mapping-by-sequencing of the *lin* mutation in a *lin* × *S. pim* F_2 population to a 0.5 Mbp mapping interval on chromosome 4 containing 80 genes including *Solyc04g005320*. Reads mapping to chromosome 4 indicate a translocation in *Solyc04g005320*, which was assayed by PCR (K). The WT allele (wt) was amplified with primer-F1 and primer-R2, which bind 5′ and 3′ to the translocation site, respectively. The *lin* mutant allele (m) was amplified with primer-F3, which binds the 3′ border of the translocated sequence, and primer-R2.

(L) Semiquantitative RT-PCR of *Solyc04g005320* in WT and *lin* showing loss of *Solyc04g005320* transcript in the *lin* mutant. *UBIQUITIN* (*UBI*) was used as control.

(M) *j2*^{CR} *lin* double mutant with elongated, weakly branched inflorescences and jointless pedicel (red asterisk). Red arrowheads mark branch points.

(N) *ej2*^{CR} *lin* double mutant with long inflorescences, extremely enlarged sepals, and inner floral organ defects (inset).

(O) Simultaneous targeting of *LIN*, *J2* and *EJ2* by CRISPR/Cas9 with two single-guide RNAs. sgRNA, Target 1 and Target 2 on each respective gene model is shown. Note that sgRNA-1 targets all three genes. Black arrows indicate forward (F) and reverse (R) primers used for PCR genotyping and sequencing (see STAR Methods). Sequencing results of second-generation (T_1) transgenic *j2*^{CR} *ej2*^{CR} *lin*^{CR} triple mutant plants generated in M82 (top) and *S. pimpinellifolium* (bottom). All three genes carry homozygous mutations.

(P) CRISPR/Cas9 targeting of *LIN* in the elite cherry cultivar Sweet 100. Sequences of *lin*^{CR} allele 1 (a1) and a2 in the first-generation (T_0) *lin*^{CR} plant #1. Five reads were obtained per plant. All sequenced alleles carried mutations, including a complex rearrangement (blue font).

(Q) Representative images of Sweet 100 and Sweet 100 *lin*^{CR} T_0 #1 mutant inflorescences showing different degrees of branching.

(R, S) Quantification of flowers per inflorescence (R) and inflorescence branching events (S) for Sweet 100 and Sweet 100 *lin*^{CR} T_0 #1. N = number of inflorescences.

Bar graphs in (E, F, H, I, R, S) show means (±SEM). *P*-values determined by two-tailed, two-sample t tests. Scale bars represent 1 cm.